ÉCOLE POLYTECHNIQUE
FÉDÉRALE DE LAUSANNE

MATHICSE
Mathematics Institute of Computational Science and Engineering
School of Basic Sciences - Section of Mathematics

MATHICSE Technical Report
Nr. 10.2011
December 2011

A two-level time step technique for the partitioned solution of one-dimensional arterial networks

A.Cristiano I. Malossi, Pablo J. Blanco and Simone Deparis

http://mathicse.epfl.ch

Phone: +41 21 69 32555

Address:
EPFL - SB - MATHICSE (Bâtiment MA)
Station 8 - CH-1015 - Lausanne - Switzerland

Fax: +41 21 69 32545

A two-level time step technique for the partitioned solution of one-dimensional arterial networks

A. Cristiano I. Malossi[a,*], Pablo J. Blanco[b,c], Simone Deparis[a]

[a] *CMCS, Chair of Modelling and Scientific Computing, MATHICSE, Mathematics Institute of Computational Science and Engineering, EPFL, École Polytechnique Fédérale de Lausanne, Station 8, CH-1015, Lausanne, Switzerland*
[b] *LNCC, Laboratório Nacional de Computação Científica, Av. Getúlio Vargas 333, Quitandinha, 25651-075, Petrópolis, Brazil*
[c] *INCT-MACC, Instituto Nacional de Ciência e Tecnologia em Medicina Assistida por Computação Científica, Petrópolis, Brazil*

Abstract

In this work a numerical strategy to address the solution of the blood flow in one-dimensional arterial networks through a topology-based decomposition is presented. Such decomposition results in the local analysis of the blood flow in simple arterial segments. Hence, iterative methods are used to perform the strong coupling among the segments, which communicate through non-overlapping interfaces. Specifically, two approaches are considered to solve the associated nonlinear interface problem: (i) the Newton method and (ii) the Broyden method. Moreover, since the modeling of blood flow in compliant vessels is tackled using explicit finite element methods, we formulate the coupling problem using a two-level time stepping technique. A local (inner) time step is used to solve the local problems in single arteries, meeting thus local stability conditions, while a global (outer) time step is employed to enforce the continuity of physical quantities of interest among the one-dimensional segments. Several examples of application are presented. Firstly a study about spurious reflexions produced at interfaces as a consequence of the two-level time stepping technique is carried out. Secondly, the application of the methodologies to physiological scenarios is presented, specifically addressing the solution of the blood flow in a model of the entire arterial network.

Keywords: One-dimensional model, Arterial network, Wave propagation, Hemodynamics, Geometrical multiscale modeling, Iterative methods

1. Introduction

Numerical simulations of the cardiovascular system using a collection of simple distributed one-dimensional (1-D) — or even lumped zero-dimensional (0-D) — models have proven to be able to provide useful information under physiological and pathophysiological conditions. They give insight about the main characteristics of the flow and about the interplay among physical phenomena taking place in the systemic arteries [1, 2, 3, 4, 5, 6, 7, 8, 9].

Solving the blood flow in the entire arterial network can be addressed through different approaches, namely: (i) fully explicit, (ii) fully implicit, and (iii) mixed explicit-implicit. The fully explicit approach entails solving at each time step a trivial system of equations with information coming from the previous time step. This approach has drawbacks concerning stability due to continuity conditions at branching sites. The fully implicit implies solving at each time step an algebraic system of equations in which all the unknowns are properly coupled. Unlike the explicit approach, this is a stable approach, but may be expensive in view of the large level of coupling among degrees of freedom within arterial segments. Finally, the mixed approach makes use of a combination of explicit and implicit methods to solve the stability issues of the fully explicit still making possible to perform explicit computations within each arterial segment due to the implicit coupling among them. This mixed approach is achieved by planning a numerical method that makes use of a two-level time discretization as will be explained afterwards.

From the computational viewpoint, there are some situations in which it is convenient to split the solution process into simpler problems, for instance: (i) in cases where the available computational implementations are based on black-box codes which cannot be accessed by the user [6], or (ii) in cases in which the number of arteries grows significantly, and the computational cost increases substantially [10]. Those situations pose the problem of developing decomposition strategies to deal with the coupled problem in an iterative manner. This implies resorting to numerical methods for solving the resulting nonlinear equations corresponding to the continuity equations considered at the interfaces among arterial segments.

The decomposition of an arterial network into subdomains can be performed in different ways. A first option is to split the entire cardiovascular system into subregions

*Corresponding author
Email addresses: cristiano.malossi@epfl.ch (A. Cristiano I. Malossi), pjblanco@lncc.br (Pablo J. Blanco), simone.deparis@epfl.ch (Simone Deparis)

corresponding to specific vascular areas, for instance legs, arms, head, organs, and so on. This was the approach taken in [11]. A second option is to explore the system into the constituent arterial segments. This approach was employed in [12] and is followed in the present work.

Each arterial segment is represented by the 1-D Fluid-Structure Interaction (FSI) model developed in [6] and is fed with proper boundary conditions at both segment boundaries. The discretization is carried out using a Taylor–Galerkin approach which yields an explicit scheme to solve for the volumetric flow rate, the pressure, and the lumen area for a single pipe. Moreover, in the present work the numerical scheme presented in [6] is further extended to deal with material and geometrical spatial inhomogeneities. In addition, the compatibility conditions that arise at the discrete level to close the discrete problem are adapted to this more general situation.

Continuity conditions are imposed among arterial segments, leading to a coupled network of deformable vessels. We propose to solve iteratively this coupled problem following the ideas developed in [13] for linear problems and recently extended in [14, 15] to flow problems in rigid pipes and in [11] to hemodynamics. Previous developments of iterative techniques to couple iteratively 1-D FSI models with Taylor–Galerkin explicit numerical formulations can be found in [12]. There, the authors use a relaxed Gauss–Seidel approach that relies on a hierarchy among the local models, dictating a compatible choice of the coupling conditions (volumetric flow rate versus average pressure). The poor convergence properties and lack of flexibility in setting boundary conditions at the arterial segment interfaces of such method can create difficulties in real situations in which we need to couple hundreds of arterial segments.

In view of these problems, we resort to two alternative approaches to solve the nonlinear coupling problem: (i) the Newton method and (ii) the Broyden method. The performance of these methods is assessed through several examples of application.

Another contribution of the present work is the development of a two-level time step technique to increase computational efficiency. Firstly, we recognize an inner local time step; it is used to solve the blood flow dynamics at each arterial segment and it is in general determined by the Courant–Friedrichs–Lewy (CFL) condition. Secondly, we consider an outer global time step which is used to match the physical quantities of interest at interfaces among arterial segments. In other words, the global time step is the one responsible for enforcing the strong coupling among the segments. This approach is convenient, also when coupling 1-D and three-dimensional (3-D) FSI problems in order to reduce the number of solutions of expensive 3-D problems with very small time steps (needed by time discretization strategy of the 1-D problem).

The generation of spurious reflections at interfaces between segments as a consequence of the proposed two-level time step technique is analyzed. In this regard we unveil the dependence of these reflections upon the wavelength and upon the ratio between the local and global time steps. In addition, we propose a simple interpolation scheme to reduce the reflections at interfaces whenever the local time step is different from the global time step.

Another aspect of the formulation, specific to the Newton method, is related to the approximation of the Jacobian in the presence of the two-level time step technique. Two procedures are compared which lead to different ways of approximating the Jacobian, and therefore to different versions of the (actually inexact) Newton method: (i) Jacobian computed using a finite difference scheme and (ii) Jacobian computed using an approximated tangent problem formulation.

All the developments in the present contribution are mainly envisaged for the hemodynamics field. Therefore, besides the study of spurious reflections carried out in academic situations, the solution of an entire arterial tree model is presented to show the robustness of the strategy in a far more complex system.

This work is organized as follows. Section 2 presents the governing equations, in continuous and discrete forms, for the 1-D FSI model of a single arterial segment. Section 3 presents the global arterial network problem and corresponding coupling equations, together with the proposed iterative methods. Section 4 deals with academic applications focusing on iterations numbers and spurious reflections, while Section 5 presents a series of comparisons of the performance of the different developed alternatives in physiological scenarios. Section 6 closes this work with the final remarks.

2. 1-D FSI model equations

The 1-D FSI model provides a simplified representation of the blood flow in deformable vessels. Although incapable to give a detailed description of the full 3-D structure of the flow field (such as recirculation or wall shear stress), it can effectively describe the wave propagation phenomena due to the compliance of the wall. In this section we first describe the governing equations for the 1-D FSI model. Then we introduce a numerical discretization of the problem. Finally, we close the resulting discrete formulation with an appropriate set of compatibility conditions.

2.1. Mass and momentum conservation laws

The 1-D FSI model is derived from the incompressible Navier–Stokes equations, by making some simplifying assumptions and integrating over the cross-section of the artery $\mathrm{S}(t,z)$, being $t \in (0,T]$ the time and $z \in [0,L]$ the axial coordinate, with L the length of the vessel. The pressure on each transversal section is assumed to be constant, and the axial velocity profile $s(r)$ is imposed through the power-law relation $s(r) = \theta^{-1}(\theta+2)\left(1-r^{\theta}\right)$, where r is the relative radial coordinate and θ is a proper coefficient. This is a commonly accepted approximation (see, for instance, [16, 17]), where $\theta = 2$ leads to a parabolic velocity

profile, while $\theta = 9$ leads to a more physiological Womersley profile. The resulting state variables are

$$A(t,z) = \int_{S(t,z)} \mathrm{dS},$$
$$Q(t,z) = \int_{S(t,z)} u_{z\mathrm{F}}(t,z)\ \mathrm{dS},$$
$$P(t,z) = \frac{1}{A(t,z)} \int_{S(t,z)} p_{\mathrm{F}}(t,z)\ \mathrm{dS},$$

where A is the cross-sectional area, Q is the volumetric flow rate, $u_{z\mathrm{F}}(r)$ is the fluid axial velocity, and P is the average pressure. A straightforward derivation of the 1-D FSI model can be found in [18]. The resulting governing equations for continuity of mass and momentum are

$$\begin{cases} \dfrac{\partial A}{\partial t} + \dfrac{\partial Q}{\partial z} = 0 & \text{in } [0,L]\times(0,T], \\ \dfrac{\partial Q}{\partial t} + \dfrac{\partial}{\partial z}\left(\alpha_{\mathrm{F}}\dfrac{Q^2}{A}\right) + \dfrac{A}{\rho_{\mathrm{F}}}\dfrac{\partial P}{\partial z} & \\ \qquad + \kappa_{\mathrm{F}}\dfrac{Q}{A} = 0 & \text{in } [0,L]\times(0,T], \\ A = \overline{A}, \qquad Q = \overline{Q} & \text{in } [0,L]\times\{0\}, \end{cases} \tag{1}$$

where α_{F} and κ_{F} are the Coriolis and friction coefficients, respectively defined as

$$\alpha_{\mathrm{F}} = \frac{1}{A}\int_{S(t,z)} s(r)^2\ \mathrm{dS}, \qquad \kappa_{\mathrm{F}} = -2\pi\frac{\mu_{\mathrm{F}}}{\rho_{\mathrm{F}}}\left.\frac{\mathrm{d}s}{\mathrm{d}r}\right|_{r=1},$$

being μ_{F} the fluid viscosity and ρ_{F} the fluid density. In (1) we also provide two initial values for the area $\overline{A}$ and for the volumetric flow rate $\overline{Q}$. The initial condition for the average pressure can be retrieved from the pressure-area relation introduced in the next section.

2.2. Constitutive law of the arterial wall

The reduced Navier–Stokes equations (1) are coupled with a simple 1-D structural model for the vessel wall, which is assumed to be axial symmetric and only radial displacements are considered. This results in a pressure-area relation, which may account for several phenomena [6]. In this work we consider the elastic and viscoelastic responses of the vessel wall, since the other terms provide negligible contributions in the cardiovascular 1-D modeling context (see, for instance, [19, 20]),

$$P = \psi(A) = P_{\mathrm{ext}} + \widehat{\psi}(A) + \widetilde{\psi}(A) \quad \text{in } [0,L]\times(0,T], \tag{2}$$

being P_{ext} a reference pressure, i.e., the pressure level at which the vessel area A is equal to the reference area A_0, and

$$\widehat{\psi}(A) = \beta_{\mathrm{S}}\left(\sqrt{\frac{A}{A_0}} - 1\right), \qquad \widetilde{\psi}(A) = \gamma_{\mathrm{S}}\left(\frac{1}{A\sqrt{A}}\frac{\partial A}{\partial t}\right),$$

with

$$\beta_{\mathrm{S}} = \sqrt{\frac{\pi}{A_0}}\frac{h_{\mathrm{S}}E_{\mathrm{S}}}{1-\nu_{\mathrm{S}}^2}, \qquad \gamma_{\mathrm{S}} = \frac{T_{\mathrm{S}}\tan\phi_{\mathrm{S}}}{4\sqrt{\pi}}\frac{h_{\mathrm{S}}E_{\mathrm{S}}}{1-\nu_{\mathrm{S}}^2},$$

where h_{S}, E_{S}, and ν_{S} are the wall thickness, elastic Young modulus, and Poisson coefficient, respectively. In addition, T_{S} is the wave characteristic time (usually taken equal to the systolic period in cardiovascular applications) and ϕ_{S} is the viscoelastic angle. The 1-D FSI problem is finally closed by providing a proper set of boundary conditions. Recall that in a cardiovascular physiological range the flow regime is typically sub-critical; the eigenvalues of the hyperbolic problem have opposite sign leading to the imposition of one boundary condition on each side of the model. These conditions can be either given data (such as time-dependent flow rate or terminal absorbing condition [21]) or coupling conditions relating a certain arterial segment with the surrounding vessels. We postpone the discussion of the latter case to Section 3.

2.3. Numerical approximation

By plugging (2) into (1), we get a closed system of differential equations. On the one hand, the elastic component of the pressure-area relation is an algebraic expression and can be easily manipulated. On the other hand, the viscoelastic term depends on the temporal derivative of the area and requires a special treatment.

In the literature, several approaches have been proposed for the numerical approximation of the 1-D FSI problem, ranging from explicit discontinuous Galerkin [21], implicit finite difference [19], or implicit finite element [20] methods. Following [6], in this work we use an operator splitting technique based on an explicit second order Taylor–Galerkin discretization, where the volumetric flow rate is split into two components such that $Q = \widehat{Q} + \widetilde{Q}$, being $\widehat{Q}$ the solution of the pure elastic problem and $\widetilde{Q}$ the viscoelastic correction. The main advantage of this approach resides in its very low computational cost, due to the explicit treatment of the main terms. The global time interval $[0,T]$ is divided into several uniform subintervals $[t^n, t^{n+1}]$, with $n = 0,1,2,\ldots$, such that $t^n = n\Delta t$, Δt being the time step. On each time subinterval, we solve the 1-D FSI problem by performing two steps.

1st step (elastic response). By removing the viscoelastic component from the formulation we can write the closed system of equations in the classical conservative form as

$$\frac{\partial \widehat{\boldsymbol{U}}}{\partial t} + \frac{\partial \boldsymbol{F}(\boldsymbol{U})}{\partial z} + \boldsymbol{S}(\boldsymbol{U}) = \boldsymbol{0} \quad \text{in } [0,L]\times(0,T], \tag{3}$$

where $\boldsymbol{U} = [A,Q]^{\mathsf{T}}$ and $\widehat{\boldsymbol{U}} = [A,\widehat{Q}]^{\mathsf{T}}$ are the total and elastic conservative variables, respectively, $\boldsymbol{F} = [Q,F_2]^{\mathsf{T}}$ are the corresponding fluxes, and $\boldsymbol{S} = [0,S_2]^{\mathsf{T}}$ accounts

for the friction and the non-uniformity of the geometry and the material, with

$$F_2 = \int_{A_0}^{A} \frac{A}{\rho_{\mathrm{F}}} \frac{\partial \widehat{\psi}}{\partial A} \, \mathrm{d}A + \alpha_{\mathrm{F}} \frac{Q^2}{A},$$

$$S_2 = B_2 - \frac{\partial}{\partial A_0} \int_{A_0}^{A} \frac{A}{\rho_{\mathrm{F}}} \frac{\partial \widehat{\psi}}{\partial A} \, \mathrm{d}A \frac{\partial A_0}{\partial z} - \frac{\partial}{\partial \beta_{\mathrm{S}}} \int_{A_0}^{A} \frac{A}{\rho_{\mathrm{F}}} \frac{\partial \widehat{\psi}}{\partial A} \, \mathrm{d}A \frac{\partial \beta_{\mathrm{S}}}{\partial z},$$

being

$$B_2 = \kappa_{\mathrm{F}} \frac{Q}{A} + \frac{A}{\rho_{\mathrm{F}}} \left(\frac{\partial \widehat{\psi}}{\partial A_0} \frac{\partial A_0}{\partial z} + \frac{\partial \widehat{\psi}}{\partial \beta_{\mathrm{S}}} \frac{\partial \beta_{\mathrm{S}}}{\partial z} \right).$$

Remark 1. Since in general the only non-uniformities present in a cardiovascular setting are related to the reference area $A_0 = A_0(z)$ and to the elastic coefficient $\beta_{\mathrm{S}} = \beta_{\mathrm{S}}(z)$, for the sake of simplicity, we assume that all the other parameters are constant along the z-axis. The extension of the present formulation to other non-uniformities (e.g., α_{F}) is straightforward.

The flux $\boldsymbol{F}$ is algebraic, since it includes only the elastic part of (2). In particular,

$$F_2 = \frac{\beta_{\mathrm{S}}}{3\rho_{\mathrm{F}}\sqrt{A_0}} \left(A^{3/2} - A_0^{3/2} \right) + \alpha_{\mathrm{F}} \frac{Q^2}{A},$$

while $\boldsymbol{S}$ is

$$S_2 = \kappa_{\mathrm{F}} \frac{Q}{A} - \frac{1}{\rho_{\mathrm{F}}} (A - A_0) \frac{\partial \beta_{\mathrm{S}}}{\partial z} + \frac{3}{2\rho_{\mathrm{F}}} \left(\left(\frac{A}{A_0} \right)^{3/2} - 1 \right) \left(A_0 \frac{\partial \beta_{\mathrm{S}}}{\partial z} - \frac{\beta_{\mathrm{S}}}{2} \frac{\partial \beta_{\mathrm{S}}}{\partial z} \right).$$

The derivatives of these quantities with respect to the conservative variables are

$$\frac{\partial \boldsymbol{F}}{\partial \boldsymbol{U}} = \begin{bmatrix} 0 & 1 \\ \dfrac{\partial F_2}{\partial A} & \dfrac{\partial F_2}{\partial Q} \end{bmatrix}, \qquad \frac{\partial \boldsymbol{S}}{\partial \boldsymbol{U}} = \begin{bmatrix} 0 & 0 \\ \dfrac{\partial S_2}{\partial A} & \dfrac{\partial S_2}{\partial Q} \end{bmatrix},$$

with

$$\frac{\partial F_2}{\partial A} = \frac{\beta_{\mathrm{S}}}{2\rho_{\mathrm{F}}} \sqrt{\frac{A}{A_0}} - \alpha_{\mathrm{F}} \frac{Q^2}{A^2},$$

$$\frac{\partial F_2}{\partial Q} = 2\alpha_{\mathrm{F}} \frac{Q}{A},$$

$$\frac{\partial S_2}{\partial A} = -\kappa_{\mathrm{F}} \frac{Q}{A^2} + \frac{1}{\rho_{\mathrm{F}}} \left(\frac{\beta_{\mathrm{S}}}{2A_0} \sqrt{\frac{A}{A_0}} \right) \frac{\partial A_0}{\partial z} + \frac{1}{\rho_{\mathrm{F}}} \left(\sqrt{\frac{A}{A_0}} - 1 \right) \frac{\partial \beta_{\mathrm{S}}}{\partial z},$$

$$\frac{\partial S_2}{\partial Q} = \frac{\kappa_{\mathrm{F}}}{A}.$$

Let $\boldsymbol{U}_h$ be the discrete counterpart of $\boldsymbol{U}$, where h refers to the spatial discretization. In addition, let $\mathcal{V}_A$ and $\mathcal{V}_{\widehat{Q}}$ be two sets of piecewise linear finite element functions with adequate boundary conditions and $\mathcal{V}_A^*$ and $\mathcal{V}_{\widehat{Q}}^*$ the associated linear spaces of admissible variations. From (3) the Taylor–Galerkin formulation for the elastic problem reads: given $\boldsymbol{U}_h^n = [A_h^n, Q_h^n]^{\mathsf{T}}$, find $\widehat{\boldsymbol{U}}_h^{n+1} = [A_h^{n+1}, \widehat{Q}_h^{n+1}]^{\mathsf{T}} \in \mathcal{V}_A \otimes \mathcal{V}_{\widehat{Q}}$ such that

$$\begin{aligned} (\widehat{\boldsymbol{U}}_h^{n+1}, \varphi_h) = (\widehat{\boldsymbol{U}}_h^n, \varphi_h) + \Delta t \left(\boldsymbol{F}(\boldsymbol{U}_h^n), \frac{\partial \varphi_h}{\partial z} \right) \\ - \frac{\Delta t^2}{2} \left(\frac{\partial \boldsymbol{F}(\boldsymbol{U}_h^n)}{\partial \boldsymbol{U}} \left(\boldsymbol{S}(\boldsymbol{U}_h^n) + \frac{\partial \boldsymbol{F}(\boldsymbol{U}_h^n)}{\partial z} \right), \frac{\partial \varphi_h}{\partial z} \right) \\ + \frac{\Delta t^2}{2} \left(\frac{\partial \boldsymbol{S}(\boldsymbol{U}_h^n)}{\partial \boldsymbol{U}} \left(\boldsymbol{S}(\boldsymbol{U}_h^n) + \frac{\partial \boldsymbol{F}(\boldsymbol{U}_h^n)}{\partial z} \right), \varphi_h \right) \\ - \Delta t \left(\boldsymbol{S}(\boldsymbol{U}_h^n), \varphi_h \right), \quad \forall \varphi_h \in \mathcal{V}_A^* \otimes \mathcal{V}_{\widehat{Q}}^*. \end{aligned} \tag{4}$$

We remark that in (4) the solution of the problem for the area (mass conservation equation) is decoupled from the one for the volumetric flow rate (momentum conservation equation). At the discrete level, the numerical problem is closed by introducing two compatibility conditions, as we discuss in Section 2.4.

2nd step (viscoelastic correction). By using the mass conservation equation, we remove the time dependence from the viscoelastic wall term. The resulting problem is

$$\frac{1}{A} \frac{\partial \widetilde{Q}}{\partial t} - \frac{\partial}{\partial z} \left(\frac{\gamma_{\mathrm{S}}}{\rho_{\mathrm{F}} A^{3/2}} \frac{\partial Q}{\partial z} \right) = 0 \quad \text{in } [0, L] \times (0, T],$$

which is closed by a proper set of homogeneous boundary conditions for $\widetilde{Q}$, as we deepen later. The corresponding finite element formulation reads: given $(A_h^{n+1}, \widehat{Q}_h^{n+1}) \in \mathcal{V}_A \otimes \mathcal{V}_{\widehat{Q}}$, find $\widetilde{Q}_h^{n+1} \in \mathcal{V}_{\widetilde{Q}}$ such that

$$\begin{aligned} \left(\frac{\widetilde{Q}_h^{n+1}}{A_h^{n+1}}, \varphi_h \right) + \Delta t \left(\frac{\gamma_{\mathrm{S}}}{\rho_{\mathrm{F}} \left(A_h^{n+1} \right)^{3/2}} \frac{\partial \widetilde{Q}_h^{n+1}}{\partial z}, \frac{\partial \varphi_h}{\partial z} \right) = \\ \left(\frac{\widetilde{Q}_h^{n}}{A_h^{n+1}}, \varphi_h \right) - \Delta t \left(\frac{\gamma_{\mathrm{S}}}{\rho_{\mathrm{F}} \left(A_h^{n+1} \right)^{3/2}} \frac{\partial \widehat{Q}_h^{n+1}}{\partial z}, \frac{\partial \varphi_h}{\partial z} \right) \\ + \Delta t \left[\frac{\gamma_{\mathrm{S}}}{\rho_{\mathrm{F}} \left(A_h^{n+1} \right)^{3/2}} \frac{\partial \widehat{Q}_h^{n+1}}{\partial z} \varphi_h \right]_0^L, \quad \forall \varphi_h \in \mathcal{V}_{\widetilde{Q}}^*, \end{aligned} \tag{5}$$

where $\mathcal{V}_{\widetilde{Q}}$ is a set of piecewise linear finite element functions with adequate boundary conditions and $\mathcal{V}_{\widetilde{Q}}^*$ is the associated linear space of admissible variations. From equation (5) it is clear that we have considered homogeneous Neumann boundary conditions for $\widetilde{Q}_h^{n+1}$. Another possibility is to consider homogeneous Dirichlet boundary conditions as proposed in [6]. The former choice suits situations in which the boundary information is the area or

the pressure, while the later choice suits when the volumetric flow rate is imposed as boundary data. We remark that eventual non-uniformities related to the viscoelastic coefficient γ_S are already included in (5).

2.4. Compatibility conditions

As mentioned in Section 2.3, even if the differential problem requires only one physical boundary condition at each interface of the 1-D FSI model, the solution of the Taylor–Galerkin problem involves the computation of a full set of values for A and Q at the first and the last node. We thus need two extra relations, namely compatibility conditions, which can be recovered by extrapolating the outgoing characteristic variables. In [6] the authors provide the main ingredients of this technique for the fully uniform case. In the present work we extend that result to the case of non-uniformity of the geometry and of the material.

Let us introduce the non-conservative form of problem (3):

$$\frac{\partial \widehat{\boldsymbol{U}}}{\partial t} + \mathrm{H}\left(\boldsymbol{U}\right)\frac{\partial \boldsymbol{U}}{\partial z} + \boldsymbol{B}\left(\boldsymbol{U}\right) = \boldsymbol{0}, \tag{6}$$

where $\mathrm{H} = \partial \boldsymbol{F}/\partial \boldsymbol{U}$ and $\boldsymbol{B} = [0, B_2]^{\mathsf{T}}$ is the counterpart of $\boldsymbol{S}$. Let Λ and L be the eigenvalue and left eigenvectors matrices of H, respectively, such that $\mathrm{LHL}^{-1} = \Lambda$. In particular they read

$$\Lambda = \begin{bmatrix} \lambda_1 & 0 \\ 0 & \lambda_2 \end{bmatrix}, \quad \mathrm{L} = \varsigma \begin{bmatrix} -\lambda_2 & 1 \\ -\lambda_1 & 1 \end{bmatrix},$$

where ς can be chosen equal to $1/A$ [6] and

$$\lambda_{1,2} = \alpha_F \frac{Q}{A} \pm \sqrt{\left(\alpha_F^2 - \alpha_F\right)\left(\frac{Q}{A}\right)^2 + \frac{A}{\rho_F}\frac{\partial \widehat{\psi}}{\partial A}}.$$

We define the pseudo-characteristic variable $\boldsymbol{Z}$ as

$$\frac{\partial \boldsymbol{Z}}{\partial \boldsymbol{U}} = \mathrm{L}.$$

From (6), after some manipulations, we get

$$\mathrm{L}\frac{\partial \widehat{\boldsymbol{U}}}{\partial t} + \Lambda\left[\frac{\partial \boldsymbol{Z}}{\partial z} - \frac{\partial \mathrm{L}}{\partial z}\boldsymbol{U}\right] + \mathrm{L}\boldsymbol{B}\left(\boldsymbol{U}\right) = \boldsymbol{0}, \tag{7}$$

where $\partial \boldsymbol{Z}/\partial z = 0$ over each pseudo-characteristic and

$$\frac{\partial \mathrm{L}}{\partial z} = \varsigma \begin{bmatrix} -\dfrac{\partial \lambda_2}{\partial z} & 0 \\ -\dfrac{\partial \lambda_1}{\partial z} & 0 \end{bmatrix},$$

with

$$\begin{aligned} \frac{\partial \lambda_{1,2}}{\partial z} &= \frac{\partial \lambda_{1,2}}{\partial A_0}\frac{\partial A_0}{\partial z} + \frac{\partial \lambda_{1,2}}{\partial \beta_S}\frac{\partial \beta_S}{\partial z} \\ &= \pm \frac{\dfrac{A}{2\rho_F}\left(\dfrac{\partial^2 \widehat{\psi}}{\partial A \partial A_0}\dfrac{\partial A_0}{\partial z} + \dfrac{\partial^2 \widehat{\psi}}{\partial A \partial \beta_S}\dfrac{\partial \beta_S}{\partial z}\right)}{\sqrt{\left(\alpha_F^2 - \alpha_F\right)\left(\dfrac{Q}{A}\right)^2 + \dfrac{A}{\rho_F}\dfrac{\partial \widehat{\psi}}{\partial A}}}, \end{aligned}$$

where

$$\begin{aligned} \frac{\partial \widehat{\psi}}{\partial A} &= \frac{\beta_S}{2A_0}\left(\frac{A}{A_0}\right)^{-1/2}, \\ \frac{\partial^2 \widehat{\psi}}{\partial A \partial A_0} &= \frac{\beta_S}{(2A_0)^2}\left(\frac{A}{A_0}\right)^{-1/2}, \\ \frac{\partial^2 \widehat{\psi}}{\partial A \partial \beta_S} &= \frac{1}{2A_0}\left(\frac{A}{A_0}\right)^{-1/2}. \end{aligned}$$

By introducing the same time discretization used in the Taylor–Galerkin problem, we write (7) on the pseudo-characteristic departing from $\boldsymbol{U}_\star^n$ towards one of the two boundary sides of the 1-D segment (more generally we use the subscript $\star$ for all the quantities evaluated at the foot of the pseudo-characteristic),

$$\mathrm{L}^n \widehat{\boldsymbol{U}}^{n+1} = \mathrm{L}^n \widehat{\boldsymbol{U}}_\star^n + \Delta t\left(\Lambda^n \frac{\partial \mathrm{L}^n}{\partial z}\left(\boldsymbol{U}_\star^n\right) - \mathrm{L}^n \boldsymbol{B}\left(\boldsymbol{U}_\star^n\right)\right). \tag{8}$$

Finally, at the numerical level, we need to balance the equations to avoid the presence of fictitious boundary flows in the reference case $\boldsymbol{U}_0 = [A_0, 0]^{\mathsf{T}}$. From (8), the balanced version of the compatibility condition reads

$$\begin{aligned} \mathrm{L}^n\left(\widehat{\boldsymbol{U}}^{n+1} - \boldsymbol{U}_0\right) = \mathrm{L}^n &\left(\widehat{\boldsymbol{U}}_\star^n - \boldsymbol{U}_{0\star}\right) \\ &+ \Delta t\, \Lambda^n \frac{\partial \mathrm{L}^n}{\partial z}\left(\boldsymbol{U}_\star^n - \boldsymbol{U}_{0\star}\right) \\ &- \Delta t\, \mathrm{L}^n\left(\boldsymbol{B}\left(\boldsymbol{U}_\star^n\right) - \boldsymbol{B}\left(\boldsymbol{U}_{0\star}\right)\right). \end{aligned}$$

The full set of boundary conditions for the finite element problem is computed solving a 2×2 linear system on each side of the 1-D segment. There are four possible cases depending on the side and type of physical boundary condition applied to the model:

$$\begin{aligned} &\text{given } Q_L\text{:} && \begin{bmatrix} \mathrm{L}_{21}^n & \mathrm{L}_{22}^n \\ 0 & 1 \end{bmatrix}\begin{pmatrix} A_h^{n+1} \\ \widehat{Q}_h^{n+1} \end{pmatrix} = \begin{pmatrix} f_L \\ Q_L \end{pmatrix} && \text{in } z = 0, \\ &\text{given } Q_R\text{:} && \begin{bmatrix} \mathrm{L}_{11}^n & \mathrm{L}_{12}^n \\ 0 & 1 \end{bmatrix}\begin{pmatrix} A_h^{n+1} \\ \widehat{Q}_h^{n+1} \end{pmatrix} = \begin{pmatrix} f_R \\ Q_R \end{pmatrix} && \text{in } z = L, \\ &\text{given } A_L\text{:} && \begin{bmatrix} \mathrm{L}_{21}^n & \mathrm{L}_{22}^n \\ 1 & 0 \end{bmatrix}\begin{pmatrix} A_h^{n+1} \\ \widehat{Q}_h^{n+1} \end{pmatrix} = \begin{pmatrix} f_L \\ A_L \end{pmatrix} && \text{in } z = 0, \\ &\text{given } A_R\text{:} && \begin{bmatrix} \mathrm{L}_{11}^n & \mathrm{L}_{12}^n \\ 1 & 0 \end{bmatrix}\begin{pmatrix} A_h^{n+1} \\ \widehat{Q}_h^{n+1} \end{pmatrix} = \begin{pmatrix} f_R \\ A_R \end{pmatrix} && \text{in } z = L, \end{aligned} \tag{9}$$

where the subscripts L and R stand for left and right sides, respectively, A_L, A_R, Q_L, and Q_R are the prescribed physical boundary conditions on the two sides of the segment,

and

$$
\begin{aligned}
f_{\mathrm{L}}\left(A_h^n, Q_h^n, \widehat{Q}_h^n\right) &= \mathrm{L}_{21}^n \left(A_0 + A_\star^n - A_{0\star}\right) + \mathrm{L}_{22}^n \widehat{Q}_\star^n \\
&+ \Delta t\, \lambda_2 \left(\frac{\partial \mathrm{L}_{21}^n}{\partial z} \left(A_\star^n - A_{0\star}\right) + \frac{\partial \mathrm{L}_{22}^n}{\partial z} Q_\star^n \right) \\
&- \Delta t\, \mathrm{L}_{21}^n \left(B_1\left(\boldsymbol{U}_\star^n\right) - B_1\left(\boldsymbol{U}_{0\star}\right)\right) \\
&- \Delta t\, \mathrm{L}_{22}^n \left(B_2\left(\boldsymbol{U}_\star^n\right) - B_2\left(\boldsymbol{U}_{0\star}\right)\right), \\
f_{\mathrm{R}}\left(A_h^n, Q_h^n, \widehat{Q}_h^n\right) &= \mathrm{L}_{11}^n \left(A_0 + A_\star^n - A_{0\star}\right) + \mathrm{L}_{12}^n \widehat{Q}_\star^n \\
&+ \Delta t\, \lambda_1 \left(\frac{\partial \mathrm{L}_{11}^n}{\partial z} \left(A_\star^n - A_{0\star}\right) + \frac{\partial \mathrm{L}_{12}^n}{\partial z} Q_\star^n \right) \\
&- \Delta t\, \mathrm{L}_{11}^n \left(B_1\left(\boldsymbol{U}_\star^n\right) - B_1\left(\boldsymbol{U}_{0\star}\right)\right) \\
&- \Delta t\, \mathrm{L}_{12}^n \left(B_2\left(\boldsymbol{U}_\star^n\right) - B_2\left(\boldsymbol{U}_{0\star}\right)\right).
\end{aligned}
$$

At the discrete level, the position of the foot of the pseudo-characteristic is computed by evaluating the CFL number of the corresponding wave

$$
N_{\mathrm{L}}^{\mathrm{CFL}} = |\lambda_{2,\mathrm{L}}| \frac{\Delta t}{h}, \qquad N_{\mathrm{R}}^{\mathrm{CFL}} = |\lambda_{1,\mathrm{R}}| \frac{\Delta t}{h}.
$$

More precisely, since we use an explicit method, the CFL number is supposed to be less than one, i.e., the foot of the pseudo-characteristic is placed in the first, last respectively, finite element of the segment. Therefore, depending from the boundary side, we approximate the quantities in the foot of the pseudo-characteristic by using one of the following first order Lagrange polynomial interpolation:

$$
\begin{aligned}
\text{left:}\ \ \boldsymbol{U}_\star^n &= \left(1 - N_{\mathrm{L}}^{\mathrm{CFL}}\right) \boldsymbol{U}_h^n\big|_{z=0} + N_{\mathrm{L}}^{\mathrm{CFL}} \boldsymbol{U}_h^n\big|_{z=h}, \\
\text{right:}\ \ \boldsymbol{U}_\star^n &= \left(1 - N_{\mathrm{R}}^{\mathrm{CFL}}\right) \boldsymbol{U}_h^n\big|_{z=L} + N_{\mathrm{R}}^{\mathrm{CFL}} \boldsymbol{U}_h^n\big|_{z=L-h}.
\end{aligned}
$$

3. Coupling techniques

In this section we briefly recall from [14] the coupling equations and the numerical algorithms we use to solve a connected network of 1-D models. Then we discuss some issues related to the explicit nature of the Taylor–Galerkin scheme presented in Section 2.3; these issues are solved by introducing a two-level time step technique. With these we account for an implicit coupling of the entire 1-D network while keeping an explicit time discretization at each 1-D segment. The implicit treatment at the global level is mandatory to capture the correct flow rate and pressure wave propagation, especially in presence of branching sites and large networks. These schemes are also envisaged for the coupling of heterogeneous models in a geometrical multiscale setting, e.g., the coupling of 1-D FSI arterial networks with 3-D FSI problems. Finally, following the idea of [11], we show how to further reduce the computational cost of our approach, by combining the methodology proposed in this work with a Broyden strategy for the update of the Jacobian matrix.

3.1. Coupling equations

The solution of the 1-D problem is given in terms of averaged/integrated scalar quantities which are the volumetric flow rate Q, the area A, and the average pressure P. Equation (2) provides an univocal relation between A and P, such that the imposition of a pressure boundary condition corresponds to the imposition of an equivalent area in (9).

The coupling of different 1-D models can be addressed by employing the same approach proposed in [14] for a more general setting. Being $\mathcal{C}$ the total number of coupling nodes present inside the general network and $\mathcal{I}_c$ the number of interfaces coupled by the c-th coupling node, we impose the following coupling equations:

$$
\forall c = 1, \dots, \mathcal{C}: \quad \begin{cases} \displaystyle\sum_{i=1}^{\mathcal{I}_c} Q_{c,i} = 0, \\ \\ P_{c,1} = P_{c,i}, \qquad \forall i = 2, \dots, \mathcal{I}_c, \end{cases} \tag{10}
$$

which represent the conservation of mass and continuity of average pressure, respectively.

Remark 2. In (1), and more generally in all the equations of the 1-D model, the volumetric flow rate is assumed to be positive in the direction of the axial coordinate z (say from the left to the right of each 1-D segment). However, (10) is written for quantities evaluated at the boundaries of the 1-D model (the coupling interfaces), where it is more convenient to assume a positive flow rate in the outgoing direction.

Remark 3. In [14] equation (10) is written in terms of the average of the normal component of the traction vector. However, for 1-D problems, the same conservation equations can be satisfied by imposing directly the continuity of the pressure at the interfaces. Indeed, the average of the normal component of the traction vector is equal to $-P$ for the 1-D FSI model.

Remark 4. Equation (10) does not take into account any energy loss at bifurcations. In the literature there are several proposed models (see, for instance, [6, 22]) to include this effect, however, as demonstrated in [23, Section 3.2], their impact on the main physical quantities is negligible for this class of models.

3.2. Numerical approach

To satisfy the set of equations (10), different coupling strategies can be used, corresponding to the imposition of different quantities on the boundaries. In other words, we can set up each subproblem with different combinations of boundary data over the coupling interfaces. Three examples are provided in [14, Section 2.5]. Each strategy has a different set of coupling variables, which are the unknowns of the interface problem.

Independently from the chosen strategy, we can arrange the coupling variables of all the $\mathcal{C}$ interfaces in a global

vector $\boldsymbol{\chi}$. The coupled problem is then solved by using a nonlinear Richardson strategy

$$\boldsymbol{\chi}^{k+1} = \boldsymbol{\chi}^{k} + \delta\boldsymbol{\chi}^{k},$$

until convergence to a suitable tolerance has been achieved. The update $\delta\boldsymbol{\chi}^{k}$ is computed by using either a Newton or inexact-Newton method

$$\mathcal{J}\left(\boldsymbol{\chi}^{k}\right)\delta\boldsymbol{\chi}^{k} = -\boldsymbol{\mathcal{R}}\left(\boldsymbol{\chi}^{k}\right),$$

which requires the computation of the residual vector $\boldsymbol{\mathcal{R}}\left(\boldsymbol{\chi}^{k}\right)$ and of the Jacobian matrix $\mathcal{J}\left(\boldsymbol{\chi}^{k}\right)$ at each k-th iteration. The graph of the Jacobian matrix depends not only on the topology of the network of models, but also on the strategy used at each coupling interface. In [14, Section 3.2.1] a general and efficient procedure to assemble the Jacobian matrix is provided.

In the forthcoming sections we describe several approaches which allow to compute the Jacobian coefficients for the 1-D FSI problem, ranging from exact/approximated tangent problem formulations to finite difference methods. In addition, in Section 3.5 we describe an alternative strategy based on the update of an existing Jacobian matrix by the Broyden method.

3.3. Jacobian coefficients computation

Due to the hyperbolic nature of the problem, we can assume that a perturbation on the boundary condition imposed on one side of the 1-D segment does not have any effect on the other side during a single time step. This amounts to consider a block-diagonal structure for the Jacobian matrix. Therefore, there exist only four different cases, leading to four different Jacobian coefficient types, as described in Figure 1.

The computation of the Jacobian coefficients can be achieved by different strategies. In particular, in this work we select two different approaches. The first is to estimate the value of the coefficients by a simple finite-difference approximation. The second one is to derive the exact tangent problem formulation of the 1-D model, which leads to the analytical expression of the coefficients.

3.3.1. Finite difference approximation

Following the approach of [11, 13], we use a finite difference approximation to estimate the value of the Jacobian coefficients. Since, as shown in Figure 1, we have both pressure and volumetric flow rate derivatives, we have to consider two different cases. The value of the pressure and of the volumetric flow rate on the left boundary of the model can be expressed through the following operators:

$$P_{\mathrm{L}} = \mathcal{P}_{\mathrm{L}}\left(Q_{\mathrm{L}}\right), \qquad Q_{\mathrm{L}} = \mathcal{Q}_{\mathrm{L}}\left(P_{\mathrm{L}}\right). \tag{11}$$

The pressure and the volumetric flow rate on the right boundary are equivalently defined; for the sake of clarity, in the following we refrain from defining both left and right quantities when unnecessary. The boundary pressure operator $\mathcal{P}_{\mathrm{L}}\left(\cdot\right)$ is defined as

$$\mathcal{P}_{\mathrm{L}}\left(Q_{\mathrm{L}}^{n+1}\right) = \psi\left(A_{\mathrm{L}}^{n+1}\right) = \psi\left(\mathcal{T}_{\mathcal{G}_{\widehat{Q}_{\mathrm{L}}\mapsto A}}\left(\widehat{Q}_{\mathrm{L}}^{n+1}\right)\Big|_{\mathrm{L}}\right), \tag{12}$$

being $\mathcal{T}_{\mathcal{G}_{\widehat{Q}_{\mathrm{L}}\mapsto A}}\left(\cdot\right)$ the Taylor–Galerkin operator (see problem (4) with boundary conditions (9)) that, given the elastic volumetric flow rate on the left side of the model, returns the area along the 1-D FSI segment.

Remark 5. As mentioned in Section 2.3, when the volumetric flow rate is imposed on a side of the 1-D segment, an homogeneous Dirichlet boundary condition is applied to the same side in the viscoelastic problem (5). Therefore, the following holds in (12): $\widetilde{Q}_{\mathrm{L}} = 0$ and $Q_{\mathrm{L}} \equiv \widehat{Q}_{\mathrm{L}}$.

The boundary volumetric flow rate operator $\mathcal{Q}_{\mathrm{L}}\left(\cdot\right)$ is given by

$$\mathcal{Q}_{\mathrm{L}}\left(P_{\mathrm{L}}^{n+1}\right) = \widehat{Q}_{\mathrm{L}}^{n+1} + \widetilde{Q}_{\mathrm{L}}^{n+1}, \tag{13}$$

where the elastic contribution is defined as

$$\widehat{Q}_{\mathrm{L}}^{n+1} = \mathcal{T}_{\mathcal{G}_{A_{\mathrm{L}}\mapsto\widehat{Q}}}\left(A_{\mathrm{L}}^{n+1}\right)\Big|_{\mathrm{L}} = \mathcal{T}_{\mathcal{G}_{A_{\mathrm{L}}\mapsto\widehat{Q}}}\left(\psi^{-1}\left(P_{\mathrm{L}}^{n+1}\right)\right)\Big|_{\mathrm{L}},$$

and the viscoelastic one is

$$\widetilde{Q}_{\mathrm{L}}^{n+1} = \mathcal{V}_{\mathcal{E}_{(\widehat{Q},A)\mapsto\widetilde{Q}}}\left(\widehat{Q}^{n+1}, A^{n+1}\right)\Big|_{\mathrm{L}} =$$

$$\mathcal{V}_{\mathcal{E}_{(\widehat{Q},A)\mapsto\widetilde{Q}}}\left(\mathcal{T}_{\mathcal{G}_{A_{\mathrm{L}}\mapsto\widehat{Q}}}\left(\psi^{-1}\left(P_{\mathrm{L}}^{n+1}\right)\right), \psi^{-1}\left(P_{\mathrm{L}}^{n+1}\right)\right)\Big|_{\mathrm{L}},$$

where ψ^{-1} is the inverse of the pressure-area operator (see equation (2)), $\mathcal{T}_{\mathcal{G}_{A_{\mathrm{L}}\mapsto\widehat{Q}}}\left(\cdot\right)$ is the Taylor–Galerkin operator (see problem (4) with boundary conditions (9)) that, given the area on the left side of the model, returns the elastic volumetric flow rate along the 1-D FSI segment, and $\mathcal{V}_{\mathcal{E}_{(\widehat{Q},A)\mapsto\widetilde{Q}}}\left(\cdot,\cdot\right)$ is the viscoelastic operator (see problem (5)) that, given the elastic flow rate and the area computed with the Taylor–Galerkin scheme, returns the viscoelastic flow rate correction along the 1-D segment. Due to the differential form of the viscoelastic term, we do not have the analytical expression for the relation $A = \psi^{-1}(P)$, which is solved numerically by using the Newton method.

The finite difference formulation for the left pressure derivative (see Figure 1(a)) is

$$\frac{\partial P_{\mathrm{L}}^{n+1}}{\partial Q_{\mathrm{L}}} = \frac{\mathcal{P}_{\mathrm{L}}\left(Q_{\mathrm{L}}^{n+1} + \delta Q\right) - \mathcal{P}_{\mathrm{L}}\left(Q_{\mathrm{L}}^{n+1}\right)}{\delta Q},$$

where δQ is a properly chosen volumetric flow rate perturbation parameter. A similar result is reached for the left volumetric flow rate coefficient (see Figure 1(c))

$$\frac{\partial Q_{\mathrm{L}}^{n+1}}{\partial P_{\mathrm{L}}} = \frac{\mathcal{Q}_{\mathrm{L}}\left(P_{\mathrm{L}}^{n+1} + \delta P\right) - \mathcal{Q}_{\mathrm{L}}\left(P_{\mathrm{L}}^{n+1}\right)}{\delta P},$$

where δP is a properly chosen pressure perturbation parameter. Indeed, the main drawback of the finite difference

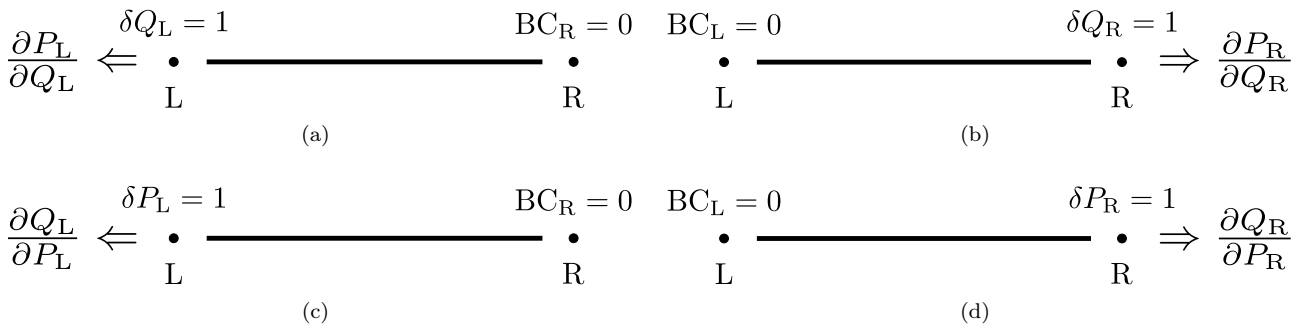

Figure 1: Scheme for the computation of the Jacobian coefficients of the 1-D model. On the top of the coupling nodes (represented by a dot) it is shown the imposed boundary condition in the case of the tangent problem formulation. The corresponding finite difference case is straightforward. BC stands for a generic boundary condition on the left/right side of the segment. (a) Computation of $\frac{\partial P_\mathrm{L}}{\partial Q_\mathrm{L}}$. (b) Computation of $\frac{\partial P_\mathrm{R}}{\partial Q_\mathrm{R}}$. (c) Computation of $\frac{\partial Q_\mathrm{L}}{\partial P_\mathrm{L}}$. (d) Computation of $\frac{\partial Q_\mathrm{R}}{\partial P_\mathrm{R}}$.

approach is that the accuracy of the approximation may depend on the choice of the perturbation parameter magnitude to be applied to the coupling quantity. In particular, when not chosen adequately, this may have a strong impact on the global convergence of the Newton scheme.

3.3.2. Exact tangent problem formulation

To overcome the limitations of the finite difference approach described in Section 3.3.1, we compute the Jacobian coefficients of the 1-D FSI model by solving the associated exact tangent problem. Deriving (12) with respect to the volumetric flow rate we get the analytical formulation of the left pressure derivative (see Figure 1(a))

$$\begin{aligned}\frac{\partial P_\mathrm{L}^{n+1}}{\partial Q_\mathrm{L}}\delta Q_\mathrm{L} &= \frac{\partial \psi\left(A_\mathrm{L}^{n+1}\right)}{\partial Q_\mathrm{L}}\delta Q_\mathrm{L} \\ &= \frac{\partial \psi\left(A_\mathrm{L}^{n+1}\right)}{\partial A_\mathrm{L}} \left.\frac{\partial \mathcal{T}_{\mathcal{G}_{\widehat{Q}_\mathrm{L}\mapsto A}}\left(\widehat{Q}_\mathrm{L}^{n+1}\right)}{\partial \widehat{Q}_\mathrm{L}}\right|_\mathrm{L} \delta Q_\mathrm{L},\end{aligned}$$

where the first term is computed by deriving (2)

$$\frac{\partial \psi\left(A^{n+1}\right)}{\partial A} = \frac{\beta_\mathrm{S}}{2\sqrt{A_0 A^{n+1}}} + \frac{\gamma_\mathrm{S}}{2\Delta t\left(A^{n+1}\right)^{3/2}}\left(3\frac{A^n}{A^{n+1}} - 1\right),$$

in which we approximate the temporal derivative of the area with a first order finite difference, and the second one is obtained from (4) and (9)

$$\left.\frac{\partial \mathcal{T}_{\mathcal{G}_{\widehat{Q}_\mathrm{L}\mapsto A}}\left(Q_\mathrm{L}^{n+1}\right)}{\partial Q_\mathrm{L}}\right|_\mathrm{L} = -\frac{\mathrm{L}_{22}}{\mathrm{L}_{21}},$$

$$\left.\frac{\partial \mathcal{T}_{\mathcal{G}_{\widehat{Q}_\mathrm{R}\mapsto A}}\left(Q_\mathrm{R}^{n+1}\right)}{\partial Q_\mathrm{R}}\right|_\mathrm{R} = -\frac{\mathrm{L}_{12}}{\mathrm{L}_{11}},$$

where we remark that the expressions for the left and right sides are different. In a similar way, deriving (13) with respect to the pressure we get the analytical formulation of the left volumetric flow rate derivatives (see Figure 1(c))

$$\frac{\partial Q_\mathrm{L}^{n+1}}{\partial P_\mathrm{L}}\delta P_\mathrm{L} = \frac{\partial \widehat{Q}_\mathrm{L}^{n+1}}{\partial P_\mathrm{L}}\delta P_\mathrm{L} + \frac{\partial \widetilde{Q}_\mathrm{L}^{n+1}}{\partial P_\mathrm{L}}\delta P_\mathrm{L},$$

where the elastic contribution is given by

$$\frac{\partial \widehat{Q}_\mathrm{L}^{n+1}}{\partial P_\mathrm{L}}\delta P_\mathrm{L} = \left.\frac{\partial \mathcal{T}_{\mathcal{G}_{A_\mathrm{L}\mapsto \widehat{Q}}}\left(A_\mathrm{L}^{n+1}\right)}{\partial A_\mathrm{L}}\right|_\mathrm{L} \frac{\partial \psi^{-1}\left(P_\mathrm{L}^{n+1}\right)}{\partial P_\mathrm{L}}\delta P_\mathrm{L},$$

where, from (4) and (9), we get

$$\left.\frac{\partial \mathcal{T}_{\mathcal{G}_{A_\mathrm{L}\mapsto \widehat{Q}}}\left(A_\mathrm{L}^{n+1}\right)}{\partial A_\mathrm{L}}\right|_\mathrm{L} = -\frac{\mathrm{L}_{21}}{\mathrm{L}_{22}},$$

$$\left.\frac{\partial \mathcal{T}_{\mathcal{G}_{A_\mathrm{R}\mapsto \widehat{Q}}}\left(A_\mathrm{R}^{n+1}\right)}{\partial A_\mathrm{R}}\right|_\mathrm{R} = -\frac{\mathrm{L}_{11}}{\mathrm{L}_{12}},$$

such that, again, the expressions for the left and right sides are not the same. The viscoelastic contribution is

$$\begin{aligned}\frac{\partial \widetilde{Q}_\mathrm{L}^{n+1}}{\partial P_\mathrm{L}}\delta P_\mathrm{L} &= \left[\frac{\partial \mathcal{V}_{\mathcal{E}_{(\widehat{Q},A)\mapsto \widetilde{Q}}}\left(\widehat{Q}^{n+1}, A^{n+1}\right)}{\partial \widehat{Q}}\frac{\partial \widehat{Q}}{\partial P_\mathrm{L}}\right]_\mathrm{L}\delta P_\mathrm{L} \\ &+ \left.\frac{\partial \mathcal{V}_{\mathcal{E}_{(\widehat{Q},A)\mapsto \widetilde{Q}}}\left(\widehat{Q}^{n+1}, A^{n+1}\right)}{\partial A_\mathrm{L}}\right|_\mathrm{L} \frac{\partial \psi^{-1}\left(P_\mathrm{L}^{n+1}\right)}{\partial P_\mathrm{L}}\delta P_\mathrm{L},\end{aligned}$$

where we remark that, at the discrete level, we have

$$\begin{aligned}&\left[\frac{\partial \mathcal{V}_{\mathcal{E}_{(\widehat{Q},A)\mapsto \widetilde{Q}}}\left(\widehat{Q}^{n+1}, A^{n+1}\right)}{\partial \widehat{Q}}\frac{\partial \widehat{Q}}{\partial P_\mathrm{L}}\right]_\mathrm{L}\delta P_\mathrm{L} \\ &= \sum_{i=1}^{n_\mathrm{FE}} \left.\frac{\partial \mathcal{V}_{\mathcal{E}_{(\widehat{Q},A)\mapsto \widetilde{Q}}}\left(\widehat{Q}^{n+1}, A^{n+1}\right)}{\partial \widehat{Q}_i}\right|_\mathrm{L} \\ &\left.\frac{\partial \mathcal{T}_{\mathcal{G}_{A_\mathrm{L}\mapsto \widehat{Q}}}\left(A_\mathrm{L}^{n+1}\right)}{\partial A_\mathrm{L}}\right|_i \frac{\partial \psi^{-1}\left(P_\mathrm{L}^{n+1}\right)}{\partial P_\mathrm{L}}\delta P_\mathrm{L},\end{aligned}$$

being n_{FE} the total number of finite element nodes used to discretize the 1-D segment. Note also that, for the reasons discussed before, the derivative of ψ^{-1} is approximated by finite differences.

3.4. Two-level time step technique

As described in Section 2.3, the 1-D problem is solved using an explicit numerical scheme. The main advantage of this approach is the very low computational cost required by the solution of the 1-D problem. However, the explicit second order Taylor–Galerkin scheme entails a strong limitation on the time step due to the CFL condition, which in this case reads [24]

$$\frac{\Delta t}{h} < \frac{\sqrt{3}}{3}.$$

This may be an issue when dealing with large networks of segments, since to perform the nonlinear Richardson iterations on the global coupled problem, the time step of all the elements of the network must be the same, i.e., the element with the most restricting time step forces the entire system to advance the computations at that time step. In particular, for the case of arterial networks, the heterogeneity of the elements is such that the difference between the required time step and the one given by the CFL condition is around two orders of magnitude, leading to a sensible increase of the computational cost. This drawback is even more visible when including some computationally expensive 3-D FSI elements in the analysis; indeed it is desirable to solve any 3-D problem as few times as possible, i.e., using a very large time step, to reduce the computational time.

In order to satisfy the CFL condition of each 1-D FSI model without imposing a global limitation on the time discretization of the other models, we devise a two-level time step technique where the inner time step meets the local 1-D CFL requirements, being different for each model, while the outer time step is used for the global coupling between the models, i.e., (10) is satisfied just at this outer level. Note that in presence of any 3-D FSI model, the outer global time step can be chosen accordingly to the requirement of the 3-D problem.

3.4.1. Inner time step interpolation

In the two-level time step approach the coupling conditions are satisfied at the outer time level. A possible way to provide the boundary conditions at the inner, and finer, time level for the 1-D FSI problems is to use interpolation. In particular, in this work we use Lagrange polynomial interpolation, whose order can be tuned to improve the final result (cf. Figure 2).

In general, in presence of large ratios between the global and the local time steps, it is expected that a linear interpolation polynomial is able to capture well long wavelength (characteristic of the arterial tree). However, in presence of short wavelengths, an inaccurate approximation of the shape of the wave during the inner time steps can generate some spurious numerical reflections at the coupling interfaces, due to the fact that (10) is satisfied just for the outer global time steps. An alternative is either to reduce the outer time step (i.e., reduce the ratio with respect to the inner time step) or to use higher order interpolation polynomials, as described with a schematic example in Figure 2.

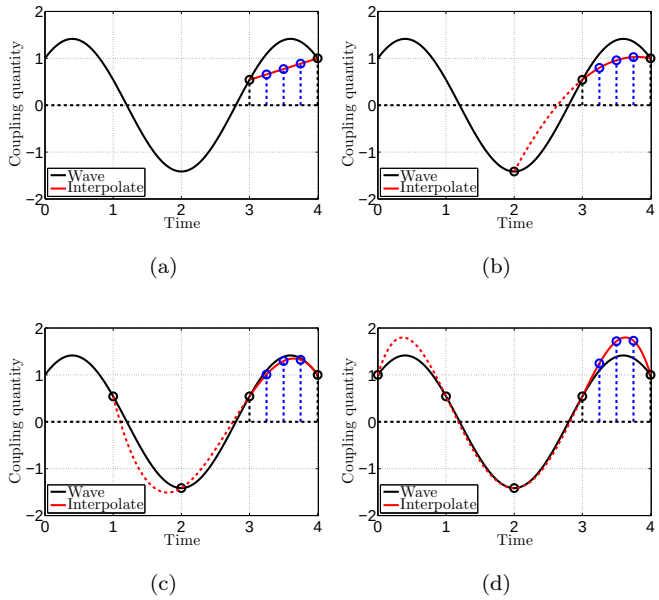

Figure 2: Two-level time step technique interpolation example: four local inner time steps (vertical dashed blue lines) are performed inside the global outer time step (vertical dashed black lines). The blue dots represent the boundary conditions imposed on the 1-D segment at each inner time step. (a) The linear interpolation does not capture the shape of the short wavelength. (b) The quadratic interpolation improves slightly the results with respect to the linear case. (c) The cubic interpolation almost capture the true shape of the wave. (d) Increasing too much the order of the interpolation may be counter-productive, as in this case for the quartic interpolation.

Further discussions and analysis about the numerical reflections are postponed to Section 4.2.

3.4.2. Jacobian coefficients approximation

The presence of inner time steps in the 1-D FSI model introduces additional difficulties in the calculation of the Jacobian coefficients. The finite difference approximation described in Section 3.3.1 is still valid, since the local inner time steps are hidden behind the pressure and volumetric flow rate operators (11). However, the analytical formulation of the tangent problem derived in Section 3.3.2 does not hold anymore, since it does not keep into account the recursion of the problem at each inner time step.

The derivation of the analytical formulation of the tangent problem for the most general case is complex and computationally expensive. Hence we devised an approximated version of the tangent problem formulation by neglecting all the recursions present in the formulation, assuming a single global time step for the approximation of the Jacobian coefficients. This is equivalent to the approach described in Section 3.3.2 with a fictitious larger time step.

As we will show in Section 4.1, both the finite difference approach and the approximated tangent formulation lead to convergent inexact-Newton schemes in simple academic cases. However, in more complex and general scenarios, like the one presented in Section 5.5, the later approach might not converge for large outer time steps.

3.5. Broyden method with matrix initialization

The computation of the Jacobian matrix at each iteration of the Newton method may be expensive from the computational viewpoint. This is even more critical when dealing with many 3-D FSI boundary interfaces, where each interface requires the solution of a 3-D FSI problem. Moreover, as discussed in the previous section, the Jacobian coefficients are approximated when using the two-level time step technique, leading to an inexact version of the Newton method, which is only linear convergent.

Following the idea in [11], we combine our approach with a Broyden strategy for the update of the Jacobian matrix [25]. More precisely, we initialize the Jacobian matrix at the first iteration of the first time step by using one of the approaches described in the previous sections. Then, for the rest of the simulation, we update the Jacobian matrix by using the Broyden method:

$$\mathcal{J}\left(\boldsymbol{\chi}^{k}\right) = \mathcal{J}\left(\boldsymbol{\chi}^{k-1}\right) + \frac{\left(\boldsymbol{\mathcal{R}}\left(\boldsymbol{\chi}^{k}\right) - \boldsymbol{\mathcal{R}}\left(\boldsymbol{\chi}^{k-1}\right)\right)\left(\delta\boldsymbol{\chi}^{k-1}\right)^{\mathsf{T}}}{\left(\delta\boldsymbol{\chi}^{k-1}\right)^{\mathsf{T}}\delta\boldsymbol{\chi}^{k-1}} - \frac{\left(\mathcal{J}\left(\boldsymbol{\chi}^{k-1}\right)\delta\boldsymbol{\chi}^{k-1}\right)\left(\delta\boldsymbol{\chi}^{k-1}\right)^{\mathsf{T}}}{\left(\delta\boldsymbol{\chi}^{k-1}\right)^{\mathsf{T}}\delta\boldsymbol{\chi}^{k-1}}. \tag{14}$$

Equation (14) does not require the solution of any tangent problem and it is based just on the evaluation of the residual of the interface problem, which is needed in any case by the Newton method. On the basis of these considerations, [14, Algorithm 2] can be upgraded to the version described in Algorithm 1 where Ω_j indicates the j-th model of the network and n_Ω is the total number of coupled 1-D models.

Remark 6. As suggested in [11], we also considered the orthogonalized version of the Broyden method. Nevertheless, in all our tested cases, this approach does not perform better than the classical version.

Remark 7. A simpler approach would be to initialize the Jacobian matrix with the identity matrix, in order to avoid, at all, the need of the techniques devised in the previous sections. However, this strategy leads to non-convergent schemes in all the tested cases. Moreover, the initialization of the Jacobian matrix is needed only at the very first iteration of the nonlinear Richardson algorithm, such that its impact on the global computational cost is negligible.

4. Academic examples

In this section we make use of simple academic examples to analyze the behaviour of the two-level time step technique introduced in Section 3.4.

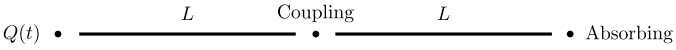

Figure 3: Schematic representation of the academic benchmark case.

To set up these analyses, we consider the benchmark case described in Figure 3, where two 1-D segments are coupled by imposing a pressure boundary data over the interfaces. This approach corresponds to satisfy (10) through the following residual formulation

$$\forall c = 1, \dots, \mathcal{C} \; : \; \boldsymbol{\mathcal{R}}_c\left(P_c, Q_{c,2}, \dots, Q_{c,\mathcal{I}_c}\right) = \mathbf{0}, \tag{15}$$

with

$$\boldsymbol{\mathcal{R}}_c = \begin{pmatrix} \mathcal{Q}_{c,1}(P_c) + \sum_{i=2}^{\mathcal{I}_c} Q_{c,i} \\ \mathcal{Q}_{c,2}(P_c) - Q_{c,2} \\ \mathcal{Q}_{c,3}(P_c) - Q_{c,3} \\ \vdots \\ \mathcal{Q}_{c,\mathcal{I}_c}(P_c) - Q_{c,\mathcal{I}_c} \end{pmatrix},$$

that is one of the three coupling strategy presented in [14, Section 2.5]. Since in a 1-D setting the solution of the coupled problem does not depend on the type of the boundary data, we do not investigate other strategies in this work. The tolerance for the iterative process is 10^{-9}. On the leftmost side we impose a given volumetric flow rate and on the rightmost one an absorbing boundary condition. The dimensionless parameters that define the problem are: $\rho_{\mathrm{F}} = 1$, $\mu_{\mathrm{F}} = 0$ (i.e., $\kappa_{\mathrm{F}} = 0$), $\alpha_{\mathrm{F}} = 1.1$, $P_{\mathrm{ext}} = 0$, $A_0 = \pi$, $h_{\mathrm{S}} = 0.1$, $E_{\mathrm{S}} = 3000000$, $\nu_{\mathrm{S}} = 0.5$ (i.e., $\beta_{\mathrm{S}} = 400000$), and $\gamma_{\mathrm{S}} = 0$. The spatial discretization h is set equal to 0.01, independently from the length L of the elements. In all the simulated cases, the inner time step is fixed to 10^{-6} and the outer time step is chosen accordingly so to control the number of inner time steps performed per each outer time step.

4.1. Iterations analysis

First of all, we study the sensitivity of the number of iterations required for the solution of the coupled problem, with respect to the number of inner time steps, the order of the Lagrange polynomial interpolation, and the applied

Algorithm 1 – Parallel time advancing with Newton & Broyden.

initialize $\boldsymbol{\chi} = \mathbf{0}$
for $t = 0, \ldots, T$
  solve $\Omega_j,\ \forall j = 1, \ldots, n_\Omega$ and compute $\boldsymbol{\mathcal{R}}(\boldsymbol{\chi})$ [parallel step]
  while $\boldsymbol{\mathcal{R}}(\boldsymbol{\chi}) \geq$ tolerance
    if at the very first nonlinear iteration
      initialize $\mathcal{J}(\boldsymbol{\chi})$ with the finite difference approximation [parallel step]
    else
      update $\mathcal{J}(\boldsymbol{\chi})$ with Broyden [parallel step]
    end
    solve $\mathcal{J}(\boldsymbol{\chi})\delta\boldsymbol{\chi} = -\boldsymbol{\mathcal{R}}(\boldsymbol{\chi})$ and update $\boldsymbol{\chi}$
    solve $\Omega_j,\ \forall j = 1, \ldots, n_\Omega$ and get $\boldsymbol{\mathcal{R}}(\boldsymbol{\chi})$ [parallel step]
  end
end

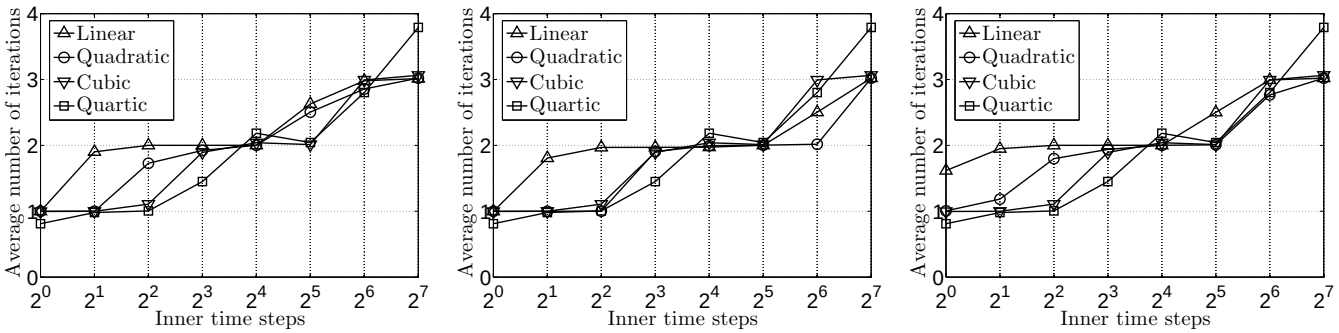

Figure 4: Average number of nonlinear Richardson iterations as a function of the number of inner time steps and of the Lagrange interpolation order. (a) Approximated tangent problem formulation. (b) Finite difference approximation. (c) Broyden method.

numerical method. For this analysis we impose a periodic flow rate wave $Q(t) = \sin(2\pi t/T_\mathrm{w})$, where $T_\mathrm{w} = 0.00512$ is the chosen wave period. The length of each 1-D segment is set equal to 3.

The number of nonlinear iterations is shown in Figure 4. We can observe that, for the selected example, there is no evident dependence of the average number of iterations from the chosen iterative method. The Broyden method and both versions of the inexact-Newton algorithm behave similarly. In all the three cases, for a small number of inner time steps per outer time step, increasing the order of the Lagrange polynomial decreases the average number of iterations. However, when the number of inner time steps per outer time step is larger than 8, the curves cross each others more than once. Finally, we can observe a slightly increase of the average number of iterations with respect to the increase in the ratio between outer and inner time steps. However, even in the worse presented case (128 inner time steps per outer time step), the average number of iterations is quite small (between three and four).

4.2. Reflections analysis

A second study regards the possible presence of numerical reflections at the coupling interfaces, which are due to the interpolation at the level of the inner time steps. For this analysis we impose a single flow rate wave defined as

$$Q(t) = \begin{cases} \sin\left(\dfrac{2\pi t}{T_\mathrm{w}}\right)^2 & t < \dfrac{T_\mathrm{w}}{2}, \\ 0 & \text{otherwise.} \end{cases}$$

The length of each 1-D element is set equal to 75, such that the longest considered wave fits in a single 1-D segment. This choice allows to easily identify the reflected wave in the first segment, after the end of the prescribed wave crosses the coupling interface.

In Figure 5(a) we can observe a clear dependence of the amplitude of the reflection with respect to the wavelength and the number of inner time steps performed per outer time step. As expected, the longest the wave, the smallest the numerical reflection. Note that the longest considered wave has a period similar to the one of the human systolic phase. Hence, as we show in the next section, in a cardiovascular setting the magnitude of the numerical reflections is negligible when considering up to 128 inner time steps, i.e., an outer time step of 10^{-3} s. Finally, in Figures 5(b) and 5(c) we can observe that, as for the number of coupling iterations, the benefits of a higher order Lagrange

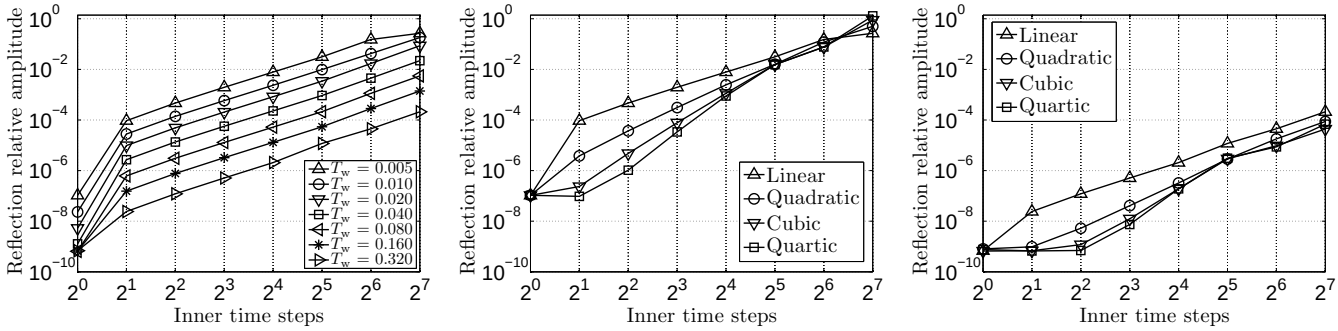

(a) (b) (c)

Figure 5: Maximum reflection relative amplitude as a function of the number of inner time steps, of the wave period, and of the Lagrange interpolation order. (a) Linear Lagrange polynomial interpolation for different wave periods. (b) Shorter tested wave period ($T_w = 0.005$) for different Lagrange interpolation orders. (c) Longer tested wave period ($T_w = 0.320$) for different Lagrange interpolation orders.

polynomial are visible only when the inner time step is close to the outer time step.

5. Modeling of the human arterial tree

In this section we apply our methodology to the arterial network provided in [19]. First of all, we recall a model for the terminal nodes of the arterial network. Then, we analyze the results, both from the modeling and the algorithmic viewpoints.

5.1. Terminals lumped parameter model

The peripheral 1-D arterial vessels are terminated with a three-element windkessel model (see Figure 6), which accounts for the cumulative effects of all distal vessels (small arteries, arterioles, and capillaries).

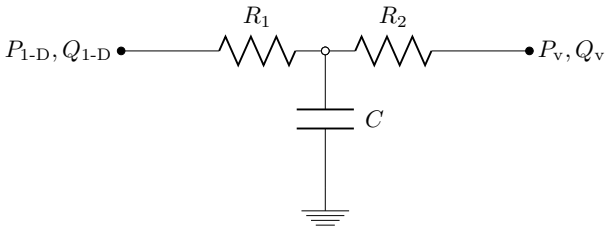

Figure 6: Three-element windkessel model.

The three-element windkessel model consists of two resistances R_1 and R_2 and a capacitor C. The values of these parameters are given by *in vivo* measurements and reasonable assumptions [19]. This model leads to a differential relation between the pressure and the volumetric flow rate in the time domain, namely

$$P_{1\text{-D}} - P_v + CR_2 \frac{\mathrm{d}P_{1\text{-D}}}{\mathrm{d}t} = (R_1 + R_2)\, Q_{1\text{-D}} + CR_1R_2 \frac{\mathrm{d}Q_{1\text{-D}}}{\mathrm{d}t}, \tag{16}$$

where $P_{1\text{-D}}$ and $Q_{1\text{-D}}$ are the pressure and the volumetric flow rate at the terminal node of the 1-D segment, respectively, and $P_v = 6666$ dyn/cm^2 is the prescribed venous pressure. Equation (16) can be solved for the pressure or for the volumetric flow rate. By introducing the approximation

$$\begin{cases} Q_{1\text{-D}}(t) \approx Q^n_{1\text{-D}} + \dfrac{Q^{n+1}_{1\text{-D}} - Q^n_{1\text{-D}}}{t^{n+1} - t^n}(t - t^n), \\ \dfrac{\mathrm{d}Q_{1\text{-D}}}{\mathrm{d}t} = \dfrac{Q^{n+1}_{1\text{-D}} - Q^n_{1\text{-D}}}{t^{n+1} - t^n}, \end{cases}$$

we can integrate (16) analytically, leading to an algebraic expression for the unknown pressure. The same approach holds when solving for the volumetric flow rate. In the following, we couple the terminal 1-D segments to the windkessel models through (15), therefore we solve (16) for the pressure.

5.2. Model predictions

The arterial model provided in [19, Figure 2 and Table 2] is composed by 103 elements (4 coronary, 24 aortic, 51 cerebral, 10 in the arms, and 14 in the legs) and includes all the values of the parameters required to describe the blood flow, such as the geometrical properties of the vessels (length and proximal/distal areas) and the data for the terminals, which are modeled as 0-D windkessel elements. These values have been obtained both from *in vivo* measurements and averaged literature data.

Regarding the parameters of the wall, since we use a different model, we estimate these values from other sources. In particular, the value of the Young modulus E_S for each arterial segment has been taken from [2] (for the body and the cerebral parts) and from [26] (for the coronaries). The Poisson ratio ν_S has been set equal to 0.5, as the arterial wall is assumed to be incompressible. The thickness of the vessels wall has been estimated equal to 10% of the local radius, which is a commonly accepted approximation,

leading to a non-uniform distribution of the coefficient β_S along the narrowed segments. Regarding the viscoelastic properties, we set the viscoelastic angle ϕ_S equal to 10° for all the vessels, while the systolic period (for the prescribed flow) is equal to 0.24 s. Note that, to enhance the comparison with the results presented in [19], we impose the same time-dependent volumetric flow rate at the inflow of the arterial network.

Finally, the other parameters that define the problem are: $\rho_F = 1.04$ g/cm^3, $\mu_F = 0.035$ g/cm/s, and $P_{ext} = 100000$ dyn/cm^2. The power law coefficient θ is set equal to 9, leading to a Womersley profile and to a value of the Coriolis coefficient of 1.1.

Figures 7 and 8 show the result of the last of seven cardiac cycles, when the periodic regime has been reached. From the analysis of the images, we can observe that the results of our simulation match the ones given in [19, Figures 4 and 5], even if some differences are present due to the different choice of the arterial wall model. Nevertheless, the predictions of our model are very accurate, especially when compared with the averaged *in vivo* measurements.

Since the validation of this model is not a matter of this work, no further comments are added here. Investigations in this direction are subject of future works.

5.3. Error analysis

To assess the accuracy of the numerical predictions of volumetric flow rate and pressure in presence of the two-level time step technique, we make a comparison with the solution of the same problem when the outer time step is equal to the inner time step, i.e., no inner time step is performed. Note that the required number of inner time steps is different for each 1-D segment, since it is computed automatically on the basis of the known value of the CFL condition and of the local properties of the element. Therefore, in order to avoid performing inner time steps in all the segments, the outer time step must be smaller enough to satisfy the CFL condition in the most restricting vessel of the network. Being $\Delta t_{2\text{-level}} = 10^{-3}$ s the global time step used for the case when the inner time step differs from the outer time step, and $\Delta t_{1\text{-level}} = 10^{-5}$ s the one chosen in order to have the outer time step equal to the most restrictive inner time step, we calculate the relative error between the two cases at each time $t^n_{2\text{-level}} = n\Delta t_{2\text{-level}}$, with $n = 0, 1, 2, \ldots$ by computing the quantities

$$\begin{aligned} \mathcal{E}_Q^{\text{mean}} &= \text{mean}(\mathcal{E}_Q)\,, \qquad \mathcal{E}_Q^{\text{max}} = \max(\mathcal{E}_Q)\,, \\ \mathcal{E}_P^{\text{mean}} &= \text{mean}(\mathcal{E}_P)\,, \qquad \mathcal{E}_P^{\text{max}} = \max(\mathcal{E}_P)\,, \end{aligned} \tag{17}$$

with

$$\mathcal{E}_Q^n = \left| \frac{Q^n_{2\text{-level}} - Q^n_{1\text{-level}}}{\max(Q_{1\text{-level}})} \right|, \qquad \mathcal{E}_P^n = \left| \frac{P^n_{2\text{-level}} - P^n_{1\text{-level}}}{P^n_{1\text{-level}}} \right|,$$

where the operators mean$(\cdot)$ and max$(\cdot)$ calculate the mean and maximum values, respectively, over all the performed time steps of the last cardiac beat.

From the analysis of the values in Table 1, we can observe that the average pressure error $\mathcal{E}_P^{\text{mean}}$ and the maximum pressure error $\mathcal{E}_P^{\text{max}}$ are always less than 0.5% and 1.0%, respectively. Regarding volumetric flow rate, the average error $\mathcal{E}_Q^{\text{mean}}$ is less than 0.5% in most of the segments, and never above 2.0%. The maximum error $\mathcal{E}_Q^{\text{max}}$ is usually around 1.0%, with a maximum of 2.5%. Increasing the order of the interpolation, the magnitude of the value does not change significantly. In view of these values, we confirm the result of Section 4.2, i.e., in a cardiovascular setting, where the wavelength are long, a linear interpolation at the level of the inner time steps leads to accurate results without significant numerical reflections.

5.4. Modeling analysis

As we already discussed in Section 2, the inclusion of the viscoelastic effect and of the local variation of the radius (and eventually of other properties) along the vessel, leads to an increase of the complexity of the model. In particular, the differential nature of the viscoelastic term requires the introduction of an operator splitting technique for the solution of the numerical problem (see Section 2.3), while the axial dependence of the reference area leads to a more complex formulation for the compatibility conditions (see Section 2.4). In view of these considerations, the reader may ask if these ingredients are really necessary to capture the true physics of the cardiovascular circulation. To answer this question, we perform a comparison between the results presented in Section 5.2 and the ones obtained removing these features from the model. In particular, we set up three cases.

Model $\mathcal{A}$. The segments in the 1-D network include both the elastic and viscoelastic wall effects. An axial linear variation of the reference radius and, consequently, of the wall thickness is present on most of the vessels.

Model $\mathcal{B}$. The segments in the 1-D network include only the elastic wall effect. An axial linear variation of the reference radius and, consequently, of the wall thickness is present on most of the vessels.

Model $\mathcal{C}$. The segments in the 1-D network include only the elastic wall effect. There is no variation of the radius and of the wall thickness in any vessel.

The results of this comparison are shown in Figure 9. As we can see, a purely elastic model of the wall (red lines) induces additional reflections along the segments, which are not dumped by the viscoelastic behavior. These reflections are further amplified when the narrowed elements are replaced by equivalent segments with a uniform reference area (blue lines). In view of this behavior, we conclude that both ingredients are mandatory for the correct prediction of the physical quantities as stated also in [19].

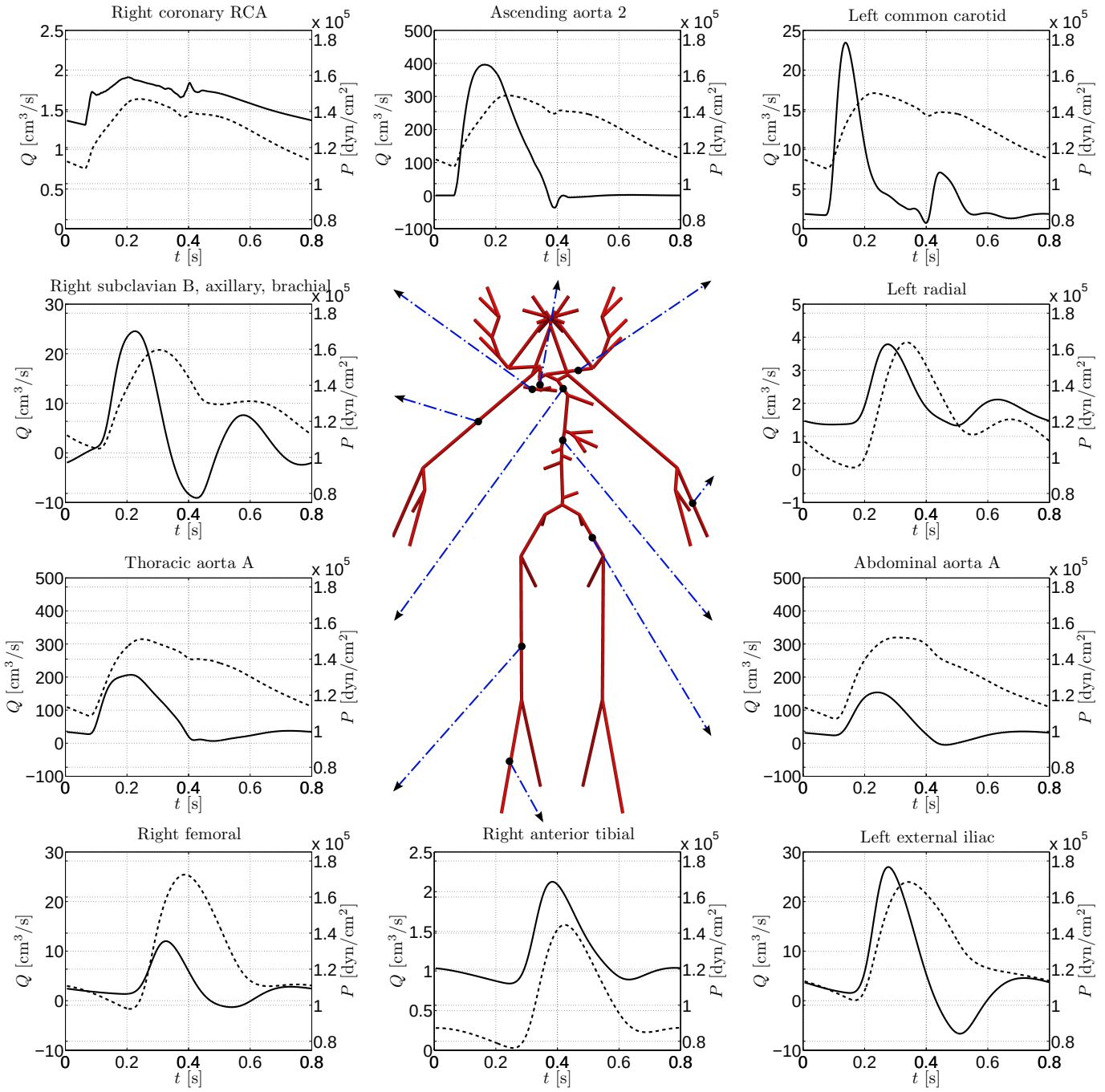

Figure 7: Periodic flow rate (solid line) and pressure (dashed line) results in ten different arterial segments. Positioning of 1-D network elements is purely visual.

5.5. Iterations analysis

In order to assess the efficiency of the methodology presented here, we compare the number of iterations required by the different algorithms to solve the full arterial network. The global coupled problem is composed of 255 interface variables. Even if this number is relatively small, it represents the implicit coupling of 150 components (103 1-D plus 47 0-D), in a complex network topology (that includes bifurcations and closed loops).

The results of this comparison are shown in Figure 10. First of all, we observe that the number of iterations required for the convergence to the solution of the global problem (up to an imposed tolerance of 10^{-6}) is always higher in the graphs in the second line (two-level time step technique, using an outer time step equal to 10^{-3} s) with respect to the ones in the first line (no inner time steps, using an outer time step equal to 10^{-5} s). This behavior is more evident for the Broyden method rather than for

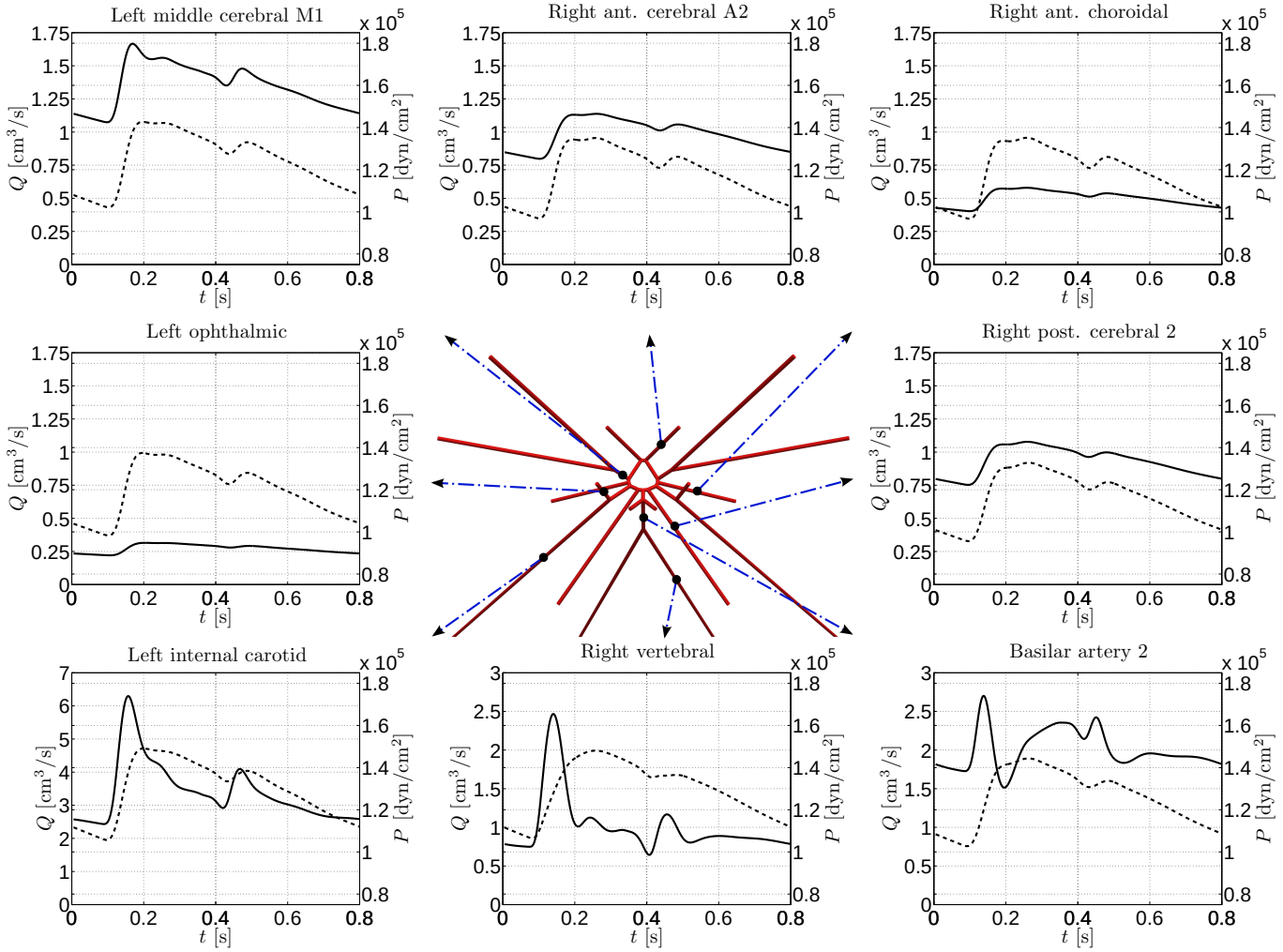

Figure 8: Periodic flow rate (solid line) and pressure (dashed line) results in eight different cerebral arterial segments. Positioning of 1-D network elements is purely visual.

the Newton method with finite difference approximation. Moreover, when the inner time step is different from the outer time step, the approximated tangent problem formulation does not converge at all.

In the second place, we also compare the results given by simplifying the model, first neglecting the viscoelastic effect (second column) and then averaging the radius along the narrowed vessels (third column). The first approximation should decrease the number of iterations, since the nonlinearities of the viscoelastic term disappear. However, comparing Figure 10(d) with Figure 10(e) we observe this behavior only during the systolic phase, while in the diastolic one the number of iterations increases. This can be justified by observing the curves in Figure 9, where the lack of the viscoelastic effect leads to the introduction of some oscillations along the network. On the contrary, averaging the radius along the vessels seems to slightly speed up the convergence.

The results of these comparisons can be further summarized by averaging the number of iterations over the entire simulation, as done in Table 2.

Comparing the results of Table 2 with the ones presented in Figure 4 we observe that even if the simulated cardiovascular network of arteries is composed by more than 100 of elements, the average number of iterations required for the solution of the global problem is almost the same of the very simple case with just two elements. This can be explained from the fact that we are dealing with hyperbolic problems in which, for the given speed of sound, the perturbations at a given coupling interface do not spread out intanstaneously throughout the network like in an elliptic problem. Therefore, the physics of the problem couples just the adjacent segments. In fact, this is the result of the block-diagonal structure of the Jacobian matrix in the Newton method. In the Broyden method the approximation of the Jacobian does not meet this block-diagonal structure, which possibly explains the increase in the number of iterations.

Table 1: Relative errors (in %) computed applying (5.3) to all the 1-D arterial segments presented in Figures 7 and 8. A linear interpolation is used for the inner time steps.

Arterial segment	$\mathcal{E}_Q^{\text{mean}}$ (%)	$\mathcal{E}_Q^{\text{max}}$ (%)	$\mathcal{E}_P^{\text{mean}}$ (%)	$\mathcal{E}_P^{\text{max}}$ (%)
Ascending aorta 2	0.019	0.134	0.405	0.493
Thoracic aorta A	0.175	0.495	0.319	0.370
Abdominal aorta A	0.238	0.496	0.275	0.335
Left common carotid	0.198	0.719	0.298	0.367
Right coronary RCA	0.290	0.612	0.324	0.480
Right subclavian B, axillary, brachial	0.229	0.586	0.142	0.246
Left radial	0.133	0.331	0.160	0.279
Left external iliac	0.297	0.993	0.188	0.332
Right femoral	0.265	0.922	0.203	0.378
Right anterior tibial	0.178	0.635	0.219	0.421
Left internal carotid	0.489	1.020	0.218	0.361
Right vertebral	0.869	1.820	0.152	0.259
Basilar artery 2	1.430	2.470	0.113	0.228
Right ant. cerebral A2	0.248	0.643	0.241	0.592
Left middle cerebral M1	0.275	0.643	0.159	0.414
Right post. cerebral 2	0.224	0.531	0.220	0.481
Right ant. choroidal	0.214	0.590	0.202	0.525
Left ophthalmic	1.810	1.970	0.231	0.562

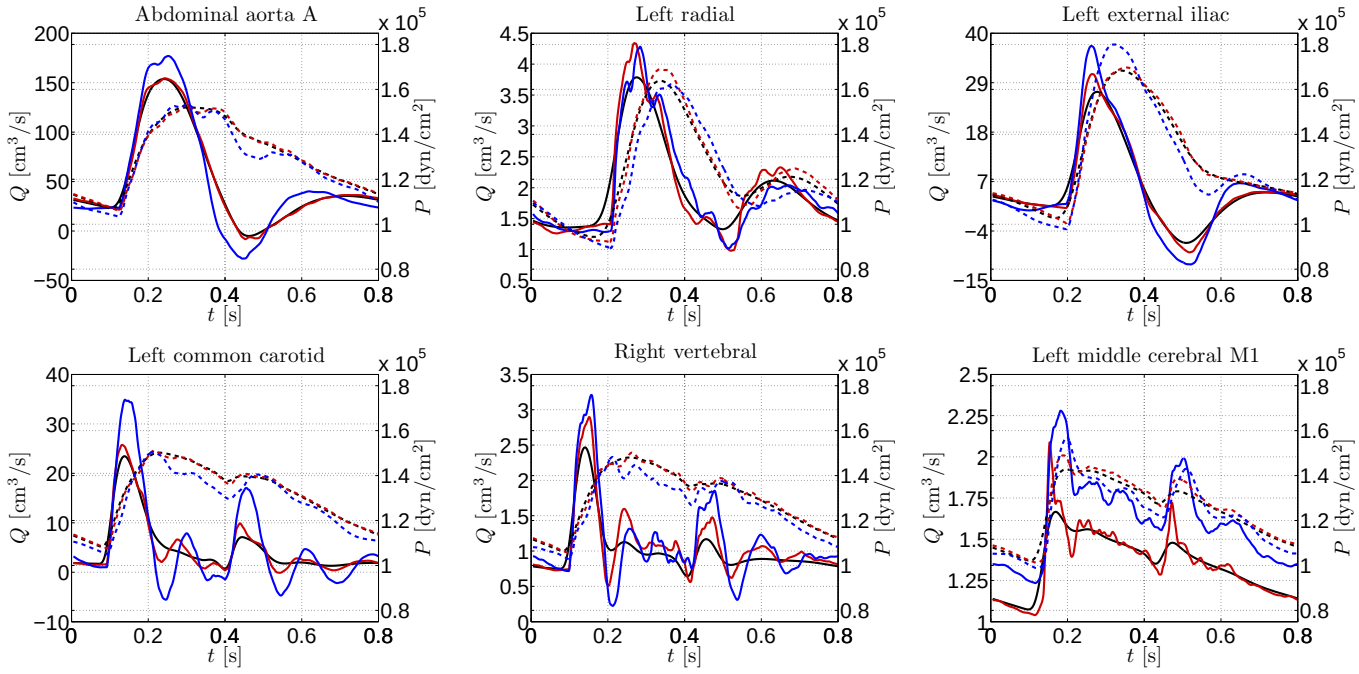

Figure 9: Comparison, in terms of physical quantities, between model $\mathcal{A}$ (black lines: same as in Figures 7 and 8), model $\mathcal{B}$ (red lines), and model $\mathcal{C}$ (blue lines) in six selected 1-D segments.

6. Conclusions

In this work, we presented a numerical technique for the partitioned solution of 1-D FSI models in arterial networks. A full description of the 1-D FSI model equations has been provided, together with the strategies used to solve the numerical problem. In particular, we extended the approaches proposed in previous works in order to include in the model some critical features such as the viscoelastic response of the arterial wall and the effect of non-uniform properties (e.g., reference area, thickness, etc.) along the vessel. The importance of these features is demonstrated by comparing the behaviour of the main

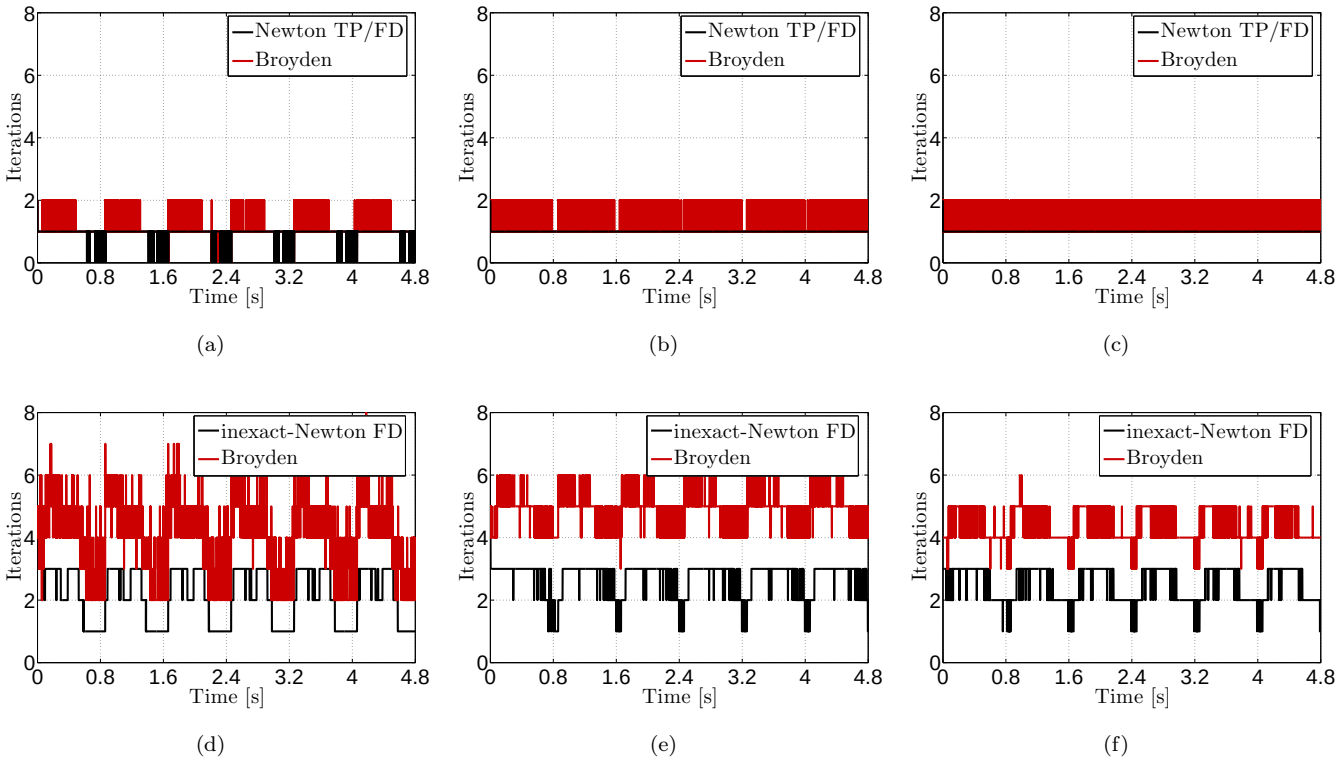

Figure 10: Comparison, in terms of number of iterations, of different algorithms for the coupling of the full 1-D arterial network. The acronyms FD and TP stand for finite difference and tangent problem, respectively. The first six heart beats are shown. (a,b,c) Cases without inner time steps. (d,e,f) Cases with inner time steps. (a,d) Model $\mathcal{A}$. (b,e) Model $\mathcal{B}$. (c,f) Model $\mathcal{C}$.

Table 2: Average number of iterations over six heart beats for different models and numerical algorithms. The acronyms FD and TP stand for finite difference and tangent problem, respectively. Note that the average number of iterations is less than one for the case of the one-level time step technique applied to model $\mathcal{A}$. This is due to the fact that, with such a low time step, it may happen that the tolerance is satisfied without any implicit iteration over the coupling quantities.

	One-level time step			Two-level time step		
Model	TP	FD	Broyden	TP	FD	Broyden
$\mathcal{A}$	0.871	0.871	0.939	–	2.107	4.024
$\mathcal{B}$	1.000	1.000	1.201	–	2.699	4.823
$\mathcal{C}$	1.000	1.000	1.253	–	2.494	4.370

physical quantities of a full 1-D arterial network with and without these ingredients.

In view of the future works involving coupling of 1-D FSI segments with other dimensionally-heterogeneous models, such as 3-D FSI models, we employed a partitioned approach for the solution of the global network of elements. Since we solve the 1-D FSI problem through an explicit algorithm, we devised a two-level time step technique for the solution of the global problem; this allows to relax the time step limitation dictated by the CFL condition in the 1-D FSI model. The problem at the coupling interfaces is solved by a classical nonlinear Richardson approach. In particular, two different numerical strategies have been selected: the Newton and the Broyden methods. The former requires the computation of the exact Jacobian matrix, which is quite complex in presence of the two-level time step technique. Therefore, two approaches for the approximation of the Jacobian have been tested, leading to inexact-Newton formulations. The latter is based just on the evaluation of the residual, leading to a very cheap formulation. Note however that the Broyden matrix needs to be initialized with a good approximation of the Jacobian, which can be obtained using one of the two inexact-Newton techniques. Recalling the expensive evaluation of the Jacobian matrix at each iteration, the Broyden method turns to be the cheapest one in terms of computational cost

per time step.

The methodology presented here has been tested on several cases, ranging from simple academic examples, consisting in serial connection of elements, to physiological applications of the entire arterial network. Indeed it has demonstrated to be robust and to perform accurately in a wide range of applications.

Acknowledgements

A. C. I. Malossi and S. Deparis acknowledge the European Research Council Advanced Grant "Mathcard, Mathematical Modelling and Simulation of the Cardiovascular System", Project ERC-2008-AdG 227058 and the Swiss Platform for High-Performance and High-Productivity Computing (HP2C). P. J. Blanco acknowledges the support of the Brazilian agencies CNPq and FAPERJ. We also acknowledge the support of the Brazilian–Swiss joint research programme (BSJRP), Project BJRP 011010 (N 590002/2010-4). We wish to thanks Luca Formaggia of Politecnico di Milano (MOX) for his precious support on the development of the 1-D solver as well as Philippe Reymond and coauthors for providing us some additional data that we used to enhance the comparison with their results (see [19]). All the numerical results presented in this paper have been computed using the `LifeV` library (www.lifev.org).

References

[1] L. Euler, Principia pro motu sanguinis per arterias determinando (1775), Opera posthuma mathematica et physica 2 (1844) 814–823.

[2] A. P. Avolio, Multi-branched model of the human arterial system, Med. Biol. Engrg. Comp. 18 (6) (1980) 709–718.

[3] J. C. Stettler, P. Niederer, M. Anliker, Theoretical analysis of arterial hemodynamics including the influence of bifurcations, part I, Ann. Biomed. Eng. 9 (1981) 145–164.

[4] N. Stergiopulos, D. F. Young, T. R. Rogge, Computer simulation of arterial flow with applications to arterial and aortic stenoses, J. Biomech. 25 (12) (1992) 1477–1488.

[5] M. S. Olufsen, Modeling the arterial system with reference to an anesthesia simulator, Ph.D. thesis, Roskilde University (May 1998).

[6] L. Formaggia, D. Lamponi, A. Quarteroni, One-dimensional models for blood flow in arteries, J. Eng. Math. 47 (3–4) (2003) 251–276.

[7] F. Liang, H. Liu, A closed-loop lumped parameter computational model for human cardiovascular system, JSME International Journal 48 (4) (2005) 484–493, series C.

[8] J. Alastruey, K. H. Parker, J. Peiró, S. M. Byrd, S. J. Sherwin, Modelling the circle of Willis to assess the effects of anatomical variations and occlusions on cerebral flows, J. Biomech. 40 (8) (2007) 1794–1805.

[9] E. Lanzarone, P. Liani, G. Baselli, M. L. Constantino, Model of arterial tree and peripheral control for the study of physiological and assisted circulation, Med. Eng. Phys. 29 (5) (2007) 542–555.

[10] J. Reichold, M. Stampanoni, A. L. Keller, A. Buck, P. Jenny, B. Weber, Vascular graph model to simulate the cerebral blood flow in realistic vascular networks, J. Cereb. Blood Flow Metab. 29 (8) (2009) 1429–1443.

[11] P. J. Blanco, J. S. Leiva, R. A. Feijóo, G. C. Buscaglia, Black-box decomposition approach for computational hemodynamics: One-dimensional models, Comp. Meth. Appl. Mech. Engrg. 200 (13–16) (2011) 1389–1405.

[12] T. Passerini, M. de Luca, L. Formaggia, A. Quarteroni, A. Veneziani, A 3D/1D geometrical multiscale model of cerebral vasculature, J. Eng. Math. 64 (4) (2009) 319–330.

[13] J. S. Leiva, P. J. Blanco, G. C. Buscaglia, Iterative strong coupling of dimensionally–heterogeneous models, Int. J. Num. Meth. Engng. 81 (12) (2010) 1558–1580.

[14] A. C. I. Malossi, P. J. Blanco, S. Deparis, A. Quarteroni, Algorithms for the partitioned solution of weakly coupled fluid models for cardiovascular flows, Int. J. Num. Meth. Biomed. Engng. 27 (12) (2011) 2035–2057.

[15] J. S. Leiva, P. J. Blanco, G. C. Buscaglia, Partitioned analysis for dimensionally-heterogeneous hydraulic networks, SIAM J. Multiscale Model. Simul. 9 (2) (2011) 872–903.

[16] N. P. Smith, A. J. Pullan, P. J. Hunter, An anatomically based model of coronary blood flow and myocardial mechanics, SIAM J. Appl. Math. 62 (2) (2002) 990–1018.

[17] A. Quarteroni, A. Veneziani, Analysis of a geometrical multiscale model based on the coupling of ode's and pde's for blood flow simulations, SIAM J. Multiscale Model. Simul. 1 (2) (2003) 173–195.

[18] A. Quarteroni, L. Formaggia, Modelling of Living Systems, Handbook of Numerical Analysis Series, Elsevier, 2003, Ch. Mathematical Modelling and Numerical Simulation of the Cardiovascular System.

[19] P. Reymond, F. Merenda, F. Perren, D. Rüfenacht, N. Stergiopulos, Validation of a one-dimensional model of the systemic arterial tree, Am. J. Physiol. Heart Circ. Physiol. 297 (1) (2009) H208–H222.

[20] P. J. Blanco, R. A. Feijóo, S. A. Urquiza, A unified variational approach for coupling 3D–1D models and its blood flow applications, Comp. Meth. Appl. Mech. Engrg. 196 (41–44) (2007) 4391–4410.

[21] S. J. Sherwin, V. Franke, J. Peiró, K. Parker, One-dimensional modelling of a vascular network in space-time variables, J. Eng. Math. 47 (3) (2003) 217–250.

[22] A. Gardel, Les pertes de charge dans les écoulements au travers de branchements en té, Tech. Rep. 10, Bulletin Technique de la Suisse Romande (1957).

[23] K. S. Matthys, J. Alastruey, J. Peiró, A. W. Khir, P. Segers, P. R. Verdonck, K. H. Parker, S. J. Sherwin, Pulse wave propagation in a model human arterial network: Assessment of 1-D numerical simulations against in vitro measurements, J. Biomech. 40 (15) (2007) 3476–3486.

[24] L. Quartapelle, Numerical Solution of the Incompressible Navier–Stokes Equations, Vol. 113 of International Series of Numerical Mathematics, Birkhäuser Verlag, Basel, 1993.

[25] C. T. Kelley, Iterative Methods for Linear and Nonlinear Equations, Frontiers in applied mathematics, SIAM, 1995.

[26] Y. Huo, G. S. Kassab, A hybrid one-dimensional/womersley model of pulsatile blood flow in the entire coronary arterial tree, Am. J. Physiol. Heart Circ. Physiol. 292 (6) (2007) H2623–H2633.

Recent publications :

MATHEMATICS INSTITUTE OF COMPUTATIONAL SCIENCE AND ENGINEERING
Section of Mathematics
Ecole Polytechnique Fédérale
CH-1015 Lausanne

19.2010 B. KALTENBACHER, M. KALTENBACHER, I. SIM:
Perfectly matched layer technique for the second order wave equations in time domain

20.2010 T. LASSILA, G. ROZZA:
Model reduction of semiaffinely parameterized partial differential equations by two-level affine approximation

21.2010 T. HOFER, J. RAPPAZ:
Numerical conservation schemes for convection-diffusion equations

22.2010 G. ROZZA, D.B. PHUONG HUYNH, A. MANZONI:
Reduced basis approximation and a posteriori error estimation for Stokes flows in parametrized geometries : roles of the inf-sup stability constants

01.2011 T. LASSILA, A. QUARTERONI, G. ROZZA:
A reduced basis model with parametric coupling for fluid-structure interaction problems

02.2011 A. QUARTERONI, G. ROZZA, A. MANZONI:
Certified Reduced Basis Approximation for Parametrized Partial Differential Equations and Applications

03.2011 M. LOMBARDI, N. PAROLINI, A.QUARTERONI, G. ROZZA:
Numerical simulation of sailing boats: dynamics, FSI and shape optimization

04.2011 P. BLANCO, P. GERVASIO, A. QUARTERONI:
Extendet variational formulation for heterogeneous partial differential equations

05.2011 A. MANZONI, A. QUARTERONI, G. ROZZA:
Model reduction techniques for fast blood flow simulation in parametrized geometries

06.2011 M. ASTORINO, J. BECERRA SAGREDO, A. QUARTERONI:
A modular lattice Boltzmann solver for GPU computing processors

07.2011 L. IAPICHINO, A. QUARTERONI, G. ROZZA:
A reduced basis hybrid method for the coupling of parametrized domains represented by fluidic networks

08.2011 T. LASSILA, A. MANZONI, G. ROZZA:
On the approximation of stability factors for general parametrized partial differential equations with a tow-level affine decomposition

09.2011 M. DISCACCIATI, A. QUARTERONI, S. QUINODOZ:
Numerical approximation of internal discontinuity interface problems

10.2011 A. C. I. MALOSSI, P. J BLANCO, S. DEPARIS:
A two-level time step technique for the partitioned solution of one-dimensional arterial networks